Fall 2018

Hes1 Notch Response Elements and their Roles in RBPJ-K Binding

Michael Majid Khayat
San Jose State University

HES1 NOTCH RESPONSE ELEMENTS AND THEIR ROLES IN RBPJ-K BINDING

A Thesis

Presented to

The Faculty of the Department of Biological Sciences

San José State University

In Partial Fulfillment

of the Requirements for the Degree

Master of Science

by

Michael Majid Khayat

December 2018

The Designated Thesis Committee Approves the Thesis Titled

HES1 NOTCH RESPONSE ELEMENTS AND THEIR ROLES IN RBPJ-K BINDING

by

Michael Majid Khayat

APPROVED FOR THE DEPARTMENT OF BIOLOGICAL SCIENCES

SAN JOSÉ STATE UNIVERSITY

December 2018

Dr. Brandon White	Department of Biological Sciences
Dr. Leila Khatib	Department of Biological Sciences
Dr. Alberto A. Rascón, Jr.	Department of Chemistry

Abstract

HES1 NOTCH RESPONSE ELEMENTS AND THEIR ROLES IN RBPJ-K BINDING

by Michael Majid Khayat

The Notch signaling pathway is a one of few fundamentally conserved signal transduction pathways critical for metazoan cellular development. Upon ligand activation, the Notch intracellular domain (NICD) translocates to the nucleus and forms a transcription complex with C-binding promoter factor-1 (RBPJ-k/CBF-1/Suppressor of Hairless) and Mastermind-like protein (MAM). The DNA-binding factor, RBPJ-k, binds to a response element containing a consensus sequence of RTGRGAR (where R is G or A). When RBPJ-k interacts with the NICD and MAM, Notch target genes are activated. The most well-characterized gene for Notch is Hes1. Hes1 contains four Notch response elements (NREs), labeled NRE 1-4. Of the four, NRE 2 and NRE 4 form what has been termed a sequence-paired site (SPS), identified as critical for transcription of Notch-dependent genes. Not all NREs are formed into an SPS, and it is hypothesized that a different transcriptional cofactor is recruited to the NREs versus the SPS to stabilize protein-DNA complexes. Base pair mutations in the Hes1 promoter were tested for binding to nuclear extract and purified RBPJ-k using an electrophoretic mobility shift assay (EMSA). Results were insufficient to determine Notch complex binding; however, the internal guanines were determined critical for RBPJ-k binding to NRE 2 and NRE 4. Additionally, despite its context in Hes1, NRE 3 also showed binding to RBPJ-k. Taken together, these results confirm that the NREs in the SPS are required for RBPJ-k structure formation and raise questions about the roles of the other single NREs.

Acknowledgements

I would like to express my most sincere recognition toward Dr. Brandon White. I am utterly honored for the research opportunity he has generously provided me. I am greatly appreciative of his knowledge in the field and high standard of research productivity. Dr. White has provided guidance to me as both a researcher and as a life mentor; I will take the experience with me for the rest of my career and life. He has taught me to never give up when obstacles present themselves, as grit will be the overcoming factor.

I would also like to thank my thesis committee members, Dr. Leila Khatib and Dr. Alberto Rascón. They have provided me with helpful feedback and suggestions throughout my graduate career and have always extended helping hands. Their input has assisted me during the completion of my M.S. program and thesis.

Thank you to Dr. Rhett Kovall for providing the purified protein used in these studies. I express my deepest gratitude to you for assisting with my thesis and also with advancements in the field. Thank you to Cassandra Ramos for the previous functionality data conducted, as this set a precedent for the structure studies presented here.

I would like to acknowledge the SJSU Department of Biological Scholarship Committee for awarding me the John and Betty Davison Research Fellowship. These funds have helped me purchase materials to aid in my research.

Finally, I would like to thank my mother, Parisa, and father, Habib, for the support system they have provided me throughout my academic career and life. Completing this thesis would not have been possible without the patience and strong working ethic they have taught me or without every form of their loving support.

Table of Contents

List of Tables

List of Figures

List of Abbreviations

ADAM:	A Disintegrin and Metalloprotease
ANK:	ankyrin
bHLH:	basic helix-loop-helix
bp:	base pairs
BTD:	β-trefoil domain
CADASIL:	cerebral autosomal dominant arteriopathy with subcortical infarcts and leukoencephalopathy
CBF-1:	C-promoter binding factor-1
CBP:	CREB binding protein
CDK8:	Cyclin-dependent kinase-8
c-Myc:	C family of Myc regulator gene
CREB:	c-AMP response element binding protein
CSL:	CBF1/Su(H)/Lag-1
CTD:	C-terminal domain
DOS:	Delta and OSM-11-like proteins
DNA:	deoxyribonucleic acid
dsDNA:	double-stranded DNA
DTT:	dithiothreitol
DSL:	Delta/Serrate/LAG-2
EGF:	Epidermal Growth Factor
EDTA:	ethylenediaminetetraacetic acid
EMSA:	electrophoretic mobility shift assay

ER:	endoplasmic reticulum
E(spl):	Enhancer of split
FBS:	fetal bovine serum
Fbw7:	Ubiquitin ligase Fbw7
GSB:	gel shift buffer
HCl:	hydrochloric acid
Hes1:	Hairy/Enhancer of Split-1:
HD:	Notch heterodimer domain
HDAC1:	Histone deacetylase-1
K_D:	dissociation binding constant
kDa:	kilodalton
LNR:	Lin12/Notch repeats
$MgCl_2$:	magnesium chloride
MAM:	Mastermind-like protein
μg:	microgram
μl:	microliter
μM:	micromolar
min:	minutes
mAmps:	milliamps
ml:	milliliter
mg:	milligram
ng:	nanogram

nM: nanomolar

NaCl: sodium chloride

NEB: nuclear extract buffer

NECD: Notch extracellular domain

NECD-NICD: Notch extracellular domain-Notch intracellular domain

NICD: Notch intracellular domain

NP-40: nonyl phenoxypolyethoxylethanol

NRE: Notch response element

NRR: negative regulatory region

NTD: N-terminal domain

O-FUT1: O-fucosyltransferase-1

PAGE: polyacrylamide gel electrophoresis

PCAF: p300/CBP-associated factor

PEST: proline, glutamate, serine, and threonine rich domain

PMSF: phenylmethane sulfonyl fluoride

PVDF: polyvinylidene difluoride

KCl: potassium chloride

polydI-dC: poly deoxyinosinic-deoxycytidylic

RAM: Recombination Binding Protein-associated module

RBPJ-k: Recombination signal Binding Protein of J-Kappa

RUMI: O-glucosyltransferase Rumi

RPM: revolutions per minute

sec:	seconds
SPS:	sequence-paired site
SupT1 NE:	SupT1 cell nuclear extract
ssDNA:	single-stranded DNA
SMRT:	Silencing mediator of retinoid and thyroid hormone receptors
TACE:	Tumor necrosis factor-α converting enzyme
TBE:	tris/borate/EDTA
TBS-T:	tris-buffered saline with Tween 20
Tris-HCl:	tris hydrochloride
TSS:	transcription starting site
V:	volts

Introduction

Notch Signaling Overview

Mammalian cellular development relies on a few well-conserved signaling pathways, which are utilized to control cellular growth and differentiation. Amidst these, the Notch signaling pathway is an important form of cell-cell communication and was first discovered in *Drosophila melanogaster* when a related mutation produced phenotypically abnormal or "notched" wings (Dexter, 1914). Nearly a century later, the pathway has become more understood with regard to the underlying genetic code and proteins that are involved within various model organisms. Disruption in this pleiotropic pathway, Notch, has been linked to a wide variety of developmental disorders and many diseases, including cancers such as T-cell acute lymphoblastic leukemia (Bray, 2006; Louvi & Artavanis-Tsakonas, 2012; Aster, Pear, & Blacklow, 2017). Ultimately the developmental outcome of Notch signaling is dependent on the context of the cell, and the signaling pathway can be suppressed or activated, influencing the cell fate in a stem-like pattern (Kopan, 2012; Kopan & Ilagan 2009). Specifically, Notch plays essential roles in epidermal development, as well as epithelial cell functions that include the endocrine and exocrine pancreatic functions (Moriyama et al., 2008; Kodama, Hijikata,, Kageyama, Shimotohno, & Chiba, 2004; Murtaugh, Stanger, Kwan, & Melton, 2003). Notch is not limited to these functions and also plays roles in vascular angiogenesis, neurological longevity, T-cell lineage commitment, and hematopoietic stem cell expansion (Kume, 2012; Gaiano, & Fishell 2002; Laky, Evans, Perez-Diez, & Fowlkes,

2015; Nobta et al., 2005). Overall, Notch plays a very general and pivotal role in multicellular development.

As species complexity increases, so does the number of genes within the organism. Mammals have evolved four Notch receptors in comparison to the one Notch receptor that is found in *Drosophila melanogaster.* The pathway is highly conserved in multicellular organisms, making it a powerful research tool for diagnosing and treating human disease. Being able to fully understand the mechanisms of activation will allow us to possibly halt the pathway in congenital diseases.

Notch and Cancer

Since the Notch pathway has a critical role in many biological processes, a dysregulation in Notch typically results in disease and abnormalities in a number of tissue types. When dysregulated, Notch can function either as a tumor suppressor or oncogene, depending on the cell context (South, Cho, & Aster 2012). Dysregulation can have an effect on a wide array of cellular functions, including the development of T-cells, and endocrine and exocrine systems. Specifically, the Hes1 gene is essential for expansion of T-cell precursors (Tomita et al., 1999); thus gene upregulation can favor leukemic cancer stem cells. Additionally, Hes1 gene expression has been correlated with the expression of stem cell markers and stemness-related genes in colon cancer cells (Gao et al., 2014; Crosnier, Stamataki, & Lewis, 2006). Hes1 plays many roles in regulating cell populations until proper differentiation signals are seen.

Overexpression of other genes affecting leukemia and colon cancers includes the upregulation of c-Myc (Smith, Mynit, & Goh, 1993). The c-Myc gene is also affected by

a gain-of-function mutation in Notch. c-Myc has been identified as an important target of Notch in the growth of leukemic cells (Weng et al., 2006). Studies have also related Notch and c-Myc to oncogenesis in breast cancer (Efstratiadis, Szabolcs, & Klinakis 2007). Due to its diverse functions, tight regulation of the Hes1 and c-Myc genes are needed for tissue-specific cell management. Notch mutations have been linked to a multitude of cancers and developmental disorders including but not limited to leukemia, solid tumors, CADASIL, and Alzheimer's disease (Louvi & Artavanis-Tsakonas, 2012; Aster et al., 2017; Berezovska et al., 1999). As Notch has a multitude of target genes, any dysregulation can lead to a number of detrimental effects during organism development.

Notch Processing

At a cellular level, Notch is a transmembrane protein that is used to communicate with neighboring cells (Kopan, 2012). The receptors are membrane-bound transcription factors that are activated upon interaction with transmembrane Notch ligands. The Notch protein is translated in the endoplasmic reticulum (ER), where it is glycosylated by enzymes O-fucosyltransferase (O-FUT1) and O-glucosyltransferase (RUMI), which are collectively responsible for ER chaperone activity and the production of a fully functional receptor (Kopan & Ilagan, 2009). The polypeptide receptor is then transported to the Golgi body, where proteolytic cleavage by furin-like convertase PC5 at site 1 (S1) results in the NECD-NICD (Notch extracellular domain-Notch intracellular domain), a heterodimer (HD) covalently held together between the N- and C-terminal ends at the HD domain. (Logeat et al., 1998; Blaumueller, Qi, Zagouras, & Artavanis-Tsakonas, 1997). These post-translational modifications then target Notch to the cell surface, where it

serves its role as a single-pass type I transmembrane protein that is activated by its ligand (Kopan & Ilagan, 2009; Blaumueller et al., 1997).

When the extracellular side of the receptor comes into contact with ligands from the Delta/Serrate/Lag-2 family, a conformational change allows for irreversible proteolytic cleavage by gamma-secretase complexes (Dexter, 1914). This leads to the release of the Notch intracellular domain which translocates to the nucleus, interacting with various proteins that initiate transcription of promoter genes. This is discussed further in the "Notch Function" section (Bray, 2006).

Notch ligands are also type I transmembrane proteins and were first identified in *Drosophila melanogaster* (D'souza, Miyamoto, & Weinmaster, 2008; Micchelli, Rufilson, & Blair, 1997). Notch is activated upon ligand specific cellular contact, where the NECD domain interacts with transmembrane protein ligands expressed on adjacent cells. The selectivity of this interaction is believed to be responsible for regulating Notch signaling in mammalian development. The NECD contains 29-36 tandem epidermal growth factor (EGF)-like repeats, which can mediate interactions with Notch ligands. The EGF is followed by a unique negative regulatory region (NRR) that contains three cysteine-rich Lin12-Notch repeats (LNR) and an HD domain (Kopan & Ilagan 2009; Sanchez-Irizarry et al., 2004). The NRR is responsible for preventing receptor activation in the absence of specific ligands, which would prematurely cleave the NECD-NICD heterodimer (Sanchez-Irizarry et al., 2004).

Notch ligands are characterized by three relating structural family motifs: the Delta/Serrate/LAG-2 (DSL) family expressed on the N-terminal of the ligand; a special

set of tandem EGF repeats that comprise the Delta and OSM-11-like proteins (DOS) family; and other EGF-like repeats, which can interact with calcium (Cordle et al., 2008; Komatsu et al., 2008). Of the DSL ligands, the Jagged/Serrate ligands are classified based on the presence of a cysteine-rich domain, which is not seen on the Delta ligands. Concurrently the DOS ligands are classified based on the presence of the DOS domain, and typically these two family of ligands are involved in receptor activation (Komatsu et al., 2008), although additional noncanonical ligands that lack both of these domains have also been reported (D'souza et al., 2008).

Mammalian Notch ligands include Delta-like 1, 3, and 4, as well as Jagged 1 and 2, which are Serrate homologs. Within the Golgi body, there is a glycosyltransferase called "Fringe." Fringe appears to be essential for Notch signaling events through its glycosylation of the Notch EGF-like repeats; it is thought this modification of the Notch ligand binding domain can decipher which ligands can activate the receptor (Munro & Freeman, 2000). In *Drosophila,* adding a single N-acetylglucosamine on EGF repeat 12 of Notch enhances Delta receptor binding, but reduces Serrate receptor binding. Interestingly enough, even in the presence of Fringe, elimination of the fucosylation site on EGF repeat 12 led to hyperactive response to Serrate/Jagged but did not change Delta response (Xu et al., 2007; Lei, Xu, Panin, & Irvine 2003).

Upon ligand binding (Figure 1), the resulting force from ligand endocytosis is thought to allow for a conformational change to expose site 2 (S2) in the Notch HD domain (Kopan & Ilagan, 2009). The protease tumor necrosis factor-α converting enzyme (TACE) from the ADAM (A Disintegrin and Metalloprotease) family then cleaves the

Notch receptor at site S2 (Brou et al.,2000). The NICD is then dissociated from the NECD, but as an intermediate form still bound to cellular membrane. The presenilin-dependent γ-secratase complex then cleaves the transitional form of the NICD at site 3 (S3) to site 4 (S4), which ultimately releases the final NICD protein from the membrane (Wolfe & Kopan, 2007; Schroeter, Kisslinger, & Kopan, 1998; De Strooper et al., 1999). Cleavage can occur at the cellular surface or within endosomal compartments. Cleavage from the membrane creates a more stable form of the NICD.

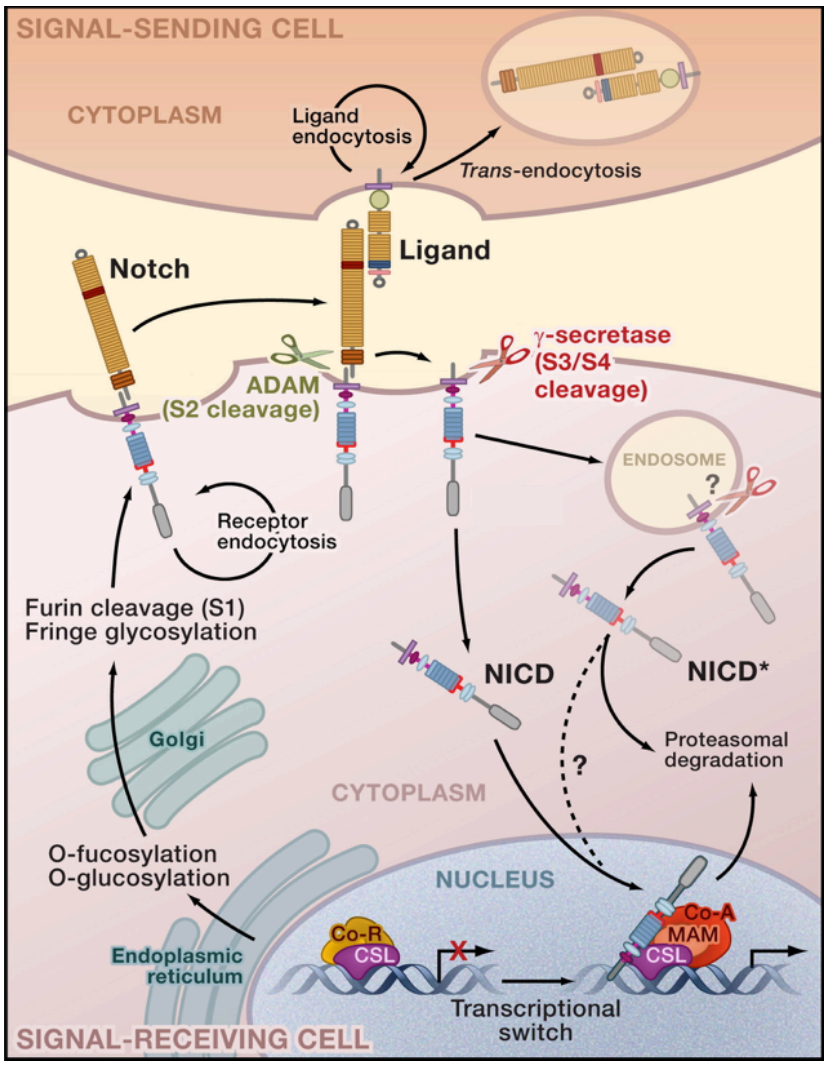

Figure 1: An overview of Notch signaling. The Notch receptor is synthesized and then undergoes essential O-fucosylation and O-glucosylation modifications. Proteolytic cleavage at site S1 will then produce a mature heterodimer receptor that will be targeted to the cell surface; Fringe modifications allow for the specificity of ligand activation. Ligand and receptor availabilities are determined by membrane trafficking and endocytosis. Ligand binding on adjacent cells is thought to cause a conformational change that will allow for ADAM cleavage at site S2, following γ-secretase cleavage at site S 3/4 at the cell surface or within the endosome. This stable form of the NICD translocates to the nucleus and interacts with DNA-binding protein CBF-1/Su(H)/Lag-1 (CSL). CSL may act as a co-repressor (Co-R) and silence genes in the absences of the NICD, although this mechanism is still under question. Transcriptional activator Mastermind (MAM) identifies this structure and recruits additional co-activators (Co-A) to activate transcription. Adapted with permission from Elsevier Ltd.: Cell (137), copyright 2009.

Notch Activation

The Notch ternary complex is in an activated state when the NICD and MAM comes into contact with RBPJ-k. Upon binding of the NICD, allosteric changes facilitate displacement of co-repressor proteins. In vertebrates, the NICD binds to the DNA-binding protein RBPJ-k, which belongs to the CSL (CBF-1/Su(H)/Lag-1) protein family. It then associates with the coactivator Mastermind-like protein (MAM), forming a ternary complex (Petcherski, & Kimble, 2000; Wu et al., 2000). Within the NICD is a Recombination Binding protein-associated module (RAM) domain, along with numerous ankyrin repeats (ANK) domain responsible for protein-protein interactions. The NICD also contains a proline, glutamate, serine, and threonine rich domain (PEST), which regulates degradation. The NICD first interacts with high affinity to RBPJ-k through the RAM domain. The ANK domain then associates with RBPJ-k to recruit MAM. This ternary complex is required for transcription by inducing the upregulation of downstream target genes (Farshbaf et al, 2015; Kovall, 2008). The binding sequence on target gene promoter is denoted as Notch response element (NRE) in these studies. This ternary complex is required to initiate transcription (Kopan & Ilagan, 2009; Kovall & Hendrickson, 2004; Borggrefe, & Oswald, 2009; Kovall & Blacklow, 2010; Kovall, Gebelein, Sprinzak, & Kopan 2017).

In absence of the NICD, RBPJ-k/CBF-1 can interact with co-repressor proteins to silence target genes (Figure 2). It is believed through interaction with corepressor complexes SMRT and histone deacetylase HDAC1, RBPJ-k silences target genes (Zhou & Hayward 2001; Kao et al., 1998; Hsieh, Zhou, Chen, Young, & Hayward, 1999;

Oswald et al., 2002). Although this is the prevailing model, recent studies have challenged the mechanism of RBPJ-k acting as a co-repressor in the absence of the NICD, as the DNA occupancy time is not as long as previously shown (VanderWielen, Yuan, Friedmann, & Kovall, 2011; Collins, Yuan, & Kovall, 2014; Gomez-Lamarca et al., 2018). This may suggest a need to reevaluate the role of RBPJ-k as co-repressor in Notch activation.

MAM has been shown to have two different roles in Notch-dependent gene regulation. When bound to the NICD and RBPJ-k, MAM has been shown to bind the general transcription factors CREB binding protein (CBP) and p300, a histone acetyltransferase critical for transcription initiation (Fryer, Lamar, Turbachova, Kintner, & Jones, 2002). With MAM present, p300/CBP-associated factor (PCAF) interacts with the NICD and acetylates chromatin exposing binding sites for other transcription factors (Wallberg, Pedersen, Lendahl, & Roeder, 2002; Fryer et al., 2002; Kurooka & Honjo, 2000). Although MAM is responsible for the linked recruitment of these transcription factors, only p300 seems to be strongly associated to MAM in the presence of the NICD. Additionally, MAM then recruits Cyclin-dependent kinase 8 (CDK8), which has been shown to phosphorylate the PEST domain of the NICD (Fryer, White, & Jones, 2004; Popko-Scibor, Lindberg, Hansson, Holmlund, & Wallberg, 2011). This phosphorylation is believed to subsequently recruit the ubiquitin ligase Fbw7, in order to poly-ubiquitinate the NICD and terminate Notch signaling (Figure 2) (Farshbaf et al., 2015).

RBPJ-k contains an N-terminal domain (NTD), a β-trefoil domain (BTD) responsible for interacting with DNA, as well as a C-terminal domain (CTD) that has no affinity for

DNA. The NICD interacts with RBPJ-K through the BTD and CTD, which bind the RAM domain and ANK repeats respectively, while the NTD interacts with C-terminal helix of MAM (Kovall & Hendrickson, 2004). Although these models set a precedent, new data have shown novel BTD-DNA interactions, and further investigation is required (Friedmann & Kovall, 2010).

A.

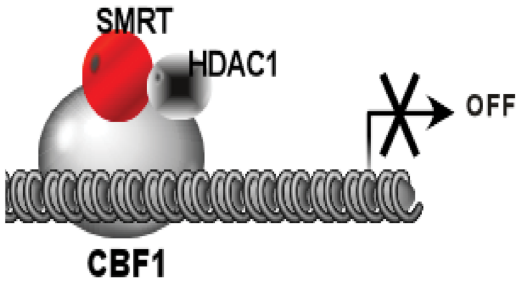

B.

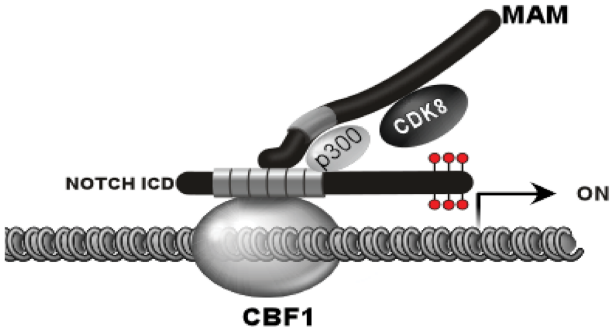

C.

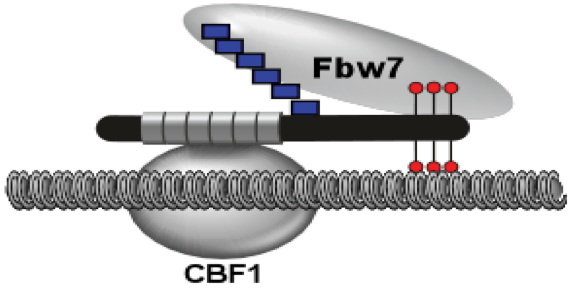

Figure 2: Notch signaling in the nucleus. (A) A proposed model of RBPJ-k/CBF-1 interacting with co-repressor SMRT and HDAC1 keeping genes turned off, although its functions remain questioned. (B) NICD translocation to the nucleus causes recruitment of MAM, p300, CDK8, and other co-activators to start transcription. CDK8 will phosphorylate the NICD in the PEST domain to signal degradation. (C) It is thought this phosphorylation, depicted here with the squares, recruits ubiquitin ligase Fbw7 to poly-ubiquinate the NICD terminating transcription. Reprinted with permission from Public Library of Science: PLOS One (10), copyright 2015.

Consensus and Non-Consensus Binding Affinity of RBPJ-k

RBPJ-k has been shown to bind a number of sequences. One consensus binding sequence that RBPJ-k recognizes with high affinity is RTGRGAR, where R is a purine nucleotide. This sequence represents some binding sites, including CGTGGGAA, and TGTGGGAA, where the underlined internal guanines are considered essential for RBPJ-k binding (Kovall & Hendrickson, 2004; Friedmann & Kovall, 2010). Other consensus sequences that may not utilize these guanines have been identified in various organisms (Tun, 1994). Previous CSL structures have shown that the BTD domain of RBPJ-k recognizes the first two underlined base pairs in the binding site TGTGGGAA. It was revealed that an absolutely conserved side chain of a glutamine and serine residue create hydrogen bonds with the purines in the T/A and G/C DNA base pairs (Figure 3) (Kovall & Hendrickson, 2004).

Not all binding sites relate to the consensus sequence and thus are termed non-consensus sites. In one such binding site, CGTGTGAA, the purine in between the internal guanines, is replaced with the underlined thymine. This T base pair in the fifth position is not seen in one binding site and is rarely seen in others. Additionally, conserved side chain reactions are seen, despite the underlined T to C base pair change seen in the first position of the binding site, CGTGTGAA (Friedmann & Kovall, 2010). Consensus and non-consensus binding sites are seen in various arrangements in different promoter genes, and they have a specific orientation within the Hes1 promoter (discussed in further detail in the "Hes1 Promoter and Sequence-Paired Sites" section). Moreover, it

has been proven that the internal guanines of the NREs are required for RBPJ-k binding (Figure 3).

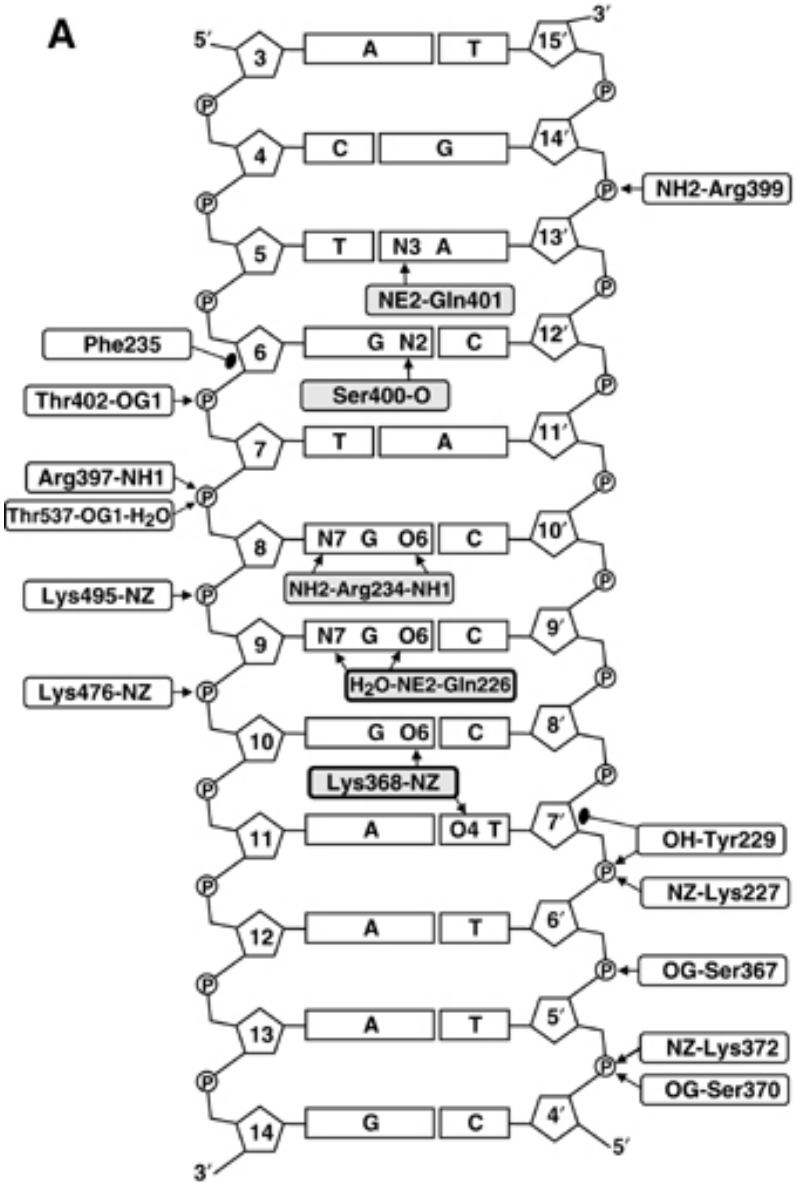

Figure 3: CSL interactions with DNA. (A) Graphic representation of all the CSL protein to consensus DNA base pair interactions. DNA bases shaded in gray indicate specific interactions; bases shaded in white indicate nonspecific interactions. Stronger bonds, such as hydrogen and salt bridges, are depicted with the arrows. Other Van der Waals forces are depicted with closed circles. Adapted with permission from European Mol. Biol. Org.: *EMBO* (23), copyright 2004.

Recent research has shown that the BTD-DNA interaction of the conserved glutamine and serine side chains are actually repositioned away from DNA. However, this still creates sufficient hydrogen bonding interactions with the T/A and G/C base pairs. Novel interactions with the minor groove of DNA have also been noted (Friedmann & Kovall, 2010). Although advances in the field are progressive, our understanding of the RBPJ-K binding structure on DNA still remains limited.

The binding affinity of the CSL proteins to the target DNA sequence has been examined by previous studies (Friedmann & Kovall, 2010; Hamaguchi, Matsunami, Yamamoto, & Honjo, 1989). In some CSL-DNA complexes, the side chains of highly conserved glutamine residues make contact with the guanine base in the major groove of DNA. The preservation of this interaction provides some insight for the selectivity and acceptance of the inner purine base pair (Kovall & Hendrickson, 2004). With this structural model in mind, it is also important to note in the non-consensus binding site of Hes1; there is a strong conservation of a thymine base pair change in place of the inner purine base pair. The idea that this inner base pair change could affect CSL protein binding led to a re-examination of recombination signal binding protein of J-Kappa (RBPJ-k) affinity to Hes1 DNA.

When measured between 5°C and 15°C, the K_D for binding of RBPJ-k to the consensus and non-consensus sites varied from 150nM to 300nM, respectively (Friedmann & Kovall, 2010). This is a 100-fold weaker affinity for DNA than what was reported before, which was 1nM (Hamaguchi et al., 1989). This moderate affinity of RBPJ-k for DNA may imply that not all RBPJ-k binding sites are occupied at all times. It

is likely that the coregulator complexes are exchanging in the nucleus, emphasizing a more cooperative mechanism of RBPJ-k recruitment to DNA sites than was previously determined. It was also discovered that mutating the inner thymine, discussed in the non-consensus site above, to a cytosine caused a reduction of binding, which increased the K_D to about 1,000nM (Friedmann & Kovall, 2010). This suggests that this inner base pair can influence the specificity and affinity of RBPJ-k to DNA, although the molecular mechanism is still in question.

Previous studies suggest that RBPJ-k has a long occupancy on DNA, repressing the target gene in the absence of the NICD. It is thought that by interacting with co-repressor complexes, RBPJ-k silences target genes (Olave, Reinberg, & Vales, 1998). This model supports the idea that the NICD competes for binding to RBPJ-k with high affinity, utilizing the RAM domain and displacing the co-repressor complexes. Recent evidence has questioned this model, as the affinity for the NICD to RBPJ-k is similar to that of the corepressors, having a disassociation constant (K_D) of around 12-15nM at 25°C (VanderWielen et al., 2011; Collins et al., 2014). New evidence also supports the idea that when the gene is silenced, RBPJ-k only transiently binds to DNA. When the gene is turned on, RBPJ-k recruitment drastically increases, as complexes reside longer on the target gene. Surprisingly, recruitment of RBPJ-k co-repressors also increased, suggesting that Notch may allow an assisted loading on target genes by providing chromatin accessibility (Gomez-Lamarca et al., 2018). RBPJ-k is critical for the structural formation of the activation complex, mediating the protein-protein interactions of the transcription factor (Wilson & Kovall, 2006; Nam, Sliz, Pear, Aster, & Blacklow 2007).

Hes1 Promoter and Sequence-Paired Sites

Of the Notch targets, the best-characterized mammalian gene is the Hes1 (Hairy enhancer of split/1) which is a homolog of *Drosophila* Hairy and Enhancer of Split (Feder, Li, Jan, & Jan, 1994; Sasai, Kageyama, Tagawa, Shigemoto, & Nakanishi, 1992). The Hes1 gene encodes for the HES1 protein, which is a nuclear protein that is a transcriptional repressor in mammals (Sasai et al., 1992). The HES1 protein belongs to the basic helix-loop-helix (bHLH) family of transcription factors, but binds to N boxes promoter regions of target genes instead of the canonical E boxes binding seen by the bHLH protein family (Blackwell, & Weintraub, 1990). HES1 binds directly to DNA and recruits repressors in *Drosophila* and mammals such as Groucho and Grg, respectively (Sasai et al., 1992), and has been associated with repressing differentiation of stem cells and progenitor cells in neural and digestive tissue types (Kageyama, Ohtsuka, & Kobayashi 2008, Kageyama, Ohtsuka, & Tomita, 2000).

The Hes1 gene has 98% homology when comparing human and murine Hes1 genes (Takebayashi et al., 1994). The transcription starting site (TSS) is upstream from the first coding region (Wu et al., 2000). Additionally, Hes1 contains four regulatory Notch response elements (NREs) upstream from the TSS. NREs on the forward DNA promoter strand are denoted as head sites; those on the reverse promoter strand are denoted as tail sites. Located farthest upstream is NRE 1, which is a tail site. It is followed by NRE 2 and NRE 3, both of which are head sites. Farthest downstream is NRE 4, orientated similar to NRE1 as a tail site.

A homolog of the Hes1 gene that has been carefully studied is the Enhancer of Split E(spl) gene in *Drosophila.* Within E(spl), two of the NREs are oriented in a specific evolutionarily conserved pattern of inverted repeats noted as a sequence-paired site (SPS) (Nellesen, Lai, & Posakony, 1999). Mutations in either of these NREs led to a less active E(spl) promoter in *Drosophila* (Cave, Loh, Surpris, Xia, & Caudy, 2005). Through these mutations it was identified that there is a specific sequence required for the activation of Notch promoter genes and ultimately Notch complex protein formation.

On Hes1, the SPS is configured on NRE 2 and NRE 4, which relate to the consensus and non-consensus binding sites, respectively (Figure 4), and is separated by about 16-17bp (Feder et al., 1994). The SPS allows Notch dimer formation and is an essential element of transcription initiation on Hes1 (Nam et al., 2007; Ong et al., 2006). NRE 2 is a head site, pointing to the right on the forward promoter strand; NRE 4 is a tail site, pointing to the left on the reverse promoter strand (Figure 4; arrows). Both the sequences "flank" each other in a specific head-to-tail orientation pattern that is important for promoter function (Ramos, 2013). It has been shown that the Notch ternary complex binds to the promoter in order to initiate mammalian transcription (Fryer et al., 2004; Ong et al., 2006). The SPS is required for promoter functionality, and research has shown that Notch dimer complexes are produced on these NREs (Cave et al., 2005, Nam et al., 2007); however our understanding of the specificity of structures recruited on different sequences is limited.

Studies have supported the idea that disrupting the SPS either through mutation, orientation, or spacing leads to less promoter activity (Ong et al., 2006). Likewise,

creating a head-to-tail site through the other NREs did not increase activity (Ramos, 2013). Within the SPS, the binding sequences of NRE 2 and NRE 4 are TGTGGGAA and CGTGTGAA, respectively, where the internal guanines are underlined. When mutating the internal guanines in NRE 2 or NRE 4, the functionality of the promoter gene is decreased, suggesting the sequence and orientation of the NREs within the SPS are critical to function. This represents the consensus and non-consensus binding sites of RBPJ-K discussed earlier, where the internal guanines are required for binding (Kovall & Hendrickson, 2004). Further examination of the NREs sequences required for RBPJ-k binding will be presented in these studies.

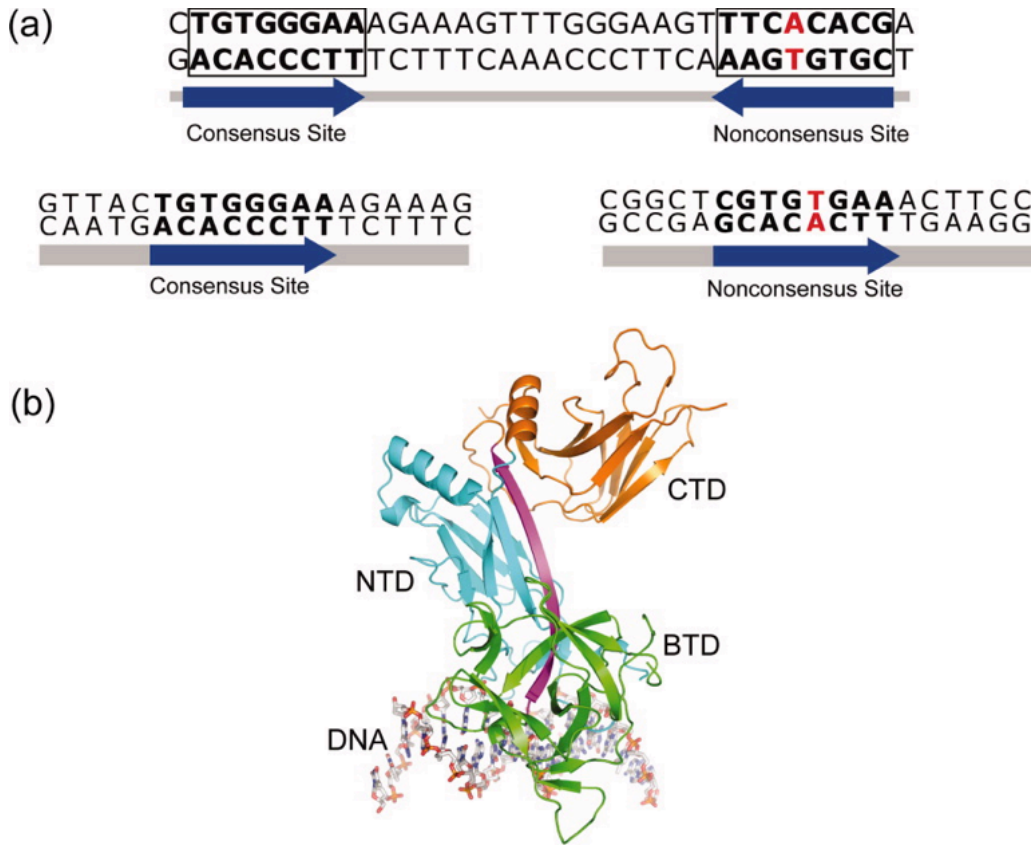

Figure 4: Hes1 SPS and the crystal structure of RBPJ-K. (A) The nucleotide sequence and graphic representation of SPS orientation in the mammalian Hes1 gene is shown. The DNA duplexes that correspond to the consensus and non-consensus sequences, read from left to right on the top strand. CSL binding sites are depicted as bold, and the T/A base pair deviation in the non-consensus strand is depicted as red. (B) The crystal structure of mouse CSL binding to the consensus sequence of DNA is represented here. The NTD, BTD, and CTD are depicted as cyan, green, and orange, respectively. Reprinted with permission from The Protein Society: *Protein Sci.* (19), copyright 2010.

Notch Dimerization

The SPS creates a response element architecture for the binding of two transcription factors. Studies have hypothesized that the head-to-tail orientation discussed earlier of NRE 2 and NRE 4 allow for structural formation of a Notch dimer, which cooperatively dimerizes on the Hes1 SPS promoter and induces transcription (Feder et al., 1994). These

studies also confirmed the crystal structure of the dimerized Notch complexes on the Hes1 promoter, forming salt bridges through the R1985A residue on the ANK domains of the NICD, conserved through a number of organisms (Figure 5) (light- and dark-blue ribbons). Transfection of a NICD construct that contains a mutated R1985A residue abolished promoter activity and dimerization (Feder et al., 1994). From these studies, it is concluded that proper structure cannot be achieved when NRE 2 or NRE 4 of the SPS orientation is disrupted, falling hand-in-hand with the decreased promoter functionality studies (Ramos, 2013; Cave et al., 2005).

Past studies have raised questions about the SPS and its importance in the Notch-MAM-CSL transcription activation complex on the Hes1 promoter. The high level of promoter activity through the SPS and Notch ternary complex dimer may suggest that another mediator may be drawn by MAM to stabilize the transcription complex on the promoter. NRE 2 and NRE 4 have been noted as critical to the SPS structure and functionality. Furthermore, it has not been determined whether any of the other NREs in the Hes1 gene are responsible for gene functionality or binding RBPJ-k; preliminary data suggest that some basal functionality can be seen when mutating the SPS (Ramos, 2013). Additionally, in *Drosophila,* Su(H) has been discovered to have a supplementary phosphorylation site on the Serine 269 residue. This residue is highly conserved and may influence interactions with the NICD or DNA (Nagel et al., 2017). Further examination in relation to RBPJ-k binding on the NRE sites within the SPS on Hes1 must be conducted; the conserved gene pathway can be a powerful tool for biomedical research once it becomes better understood.

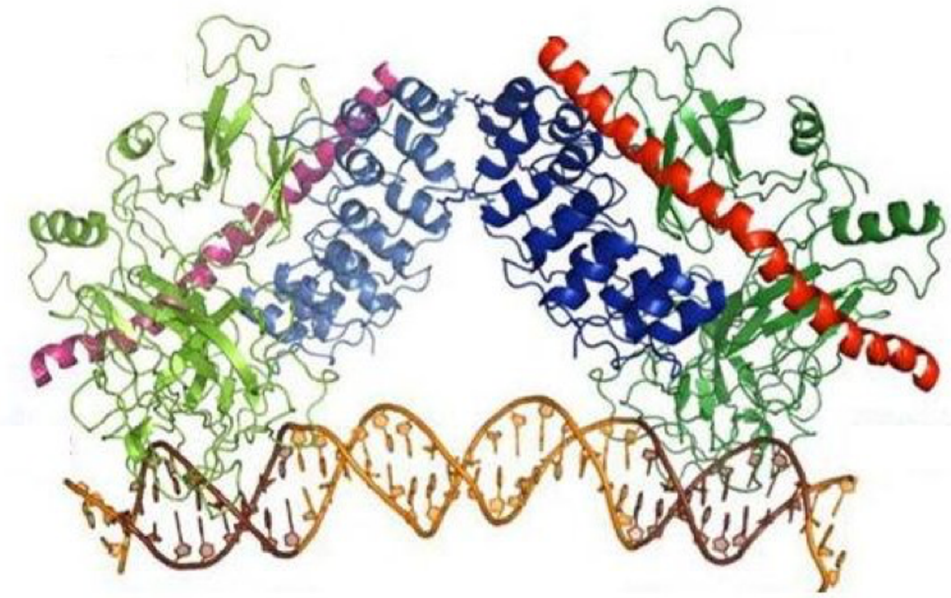

Figure 5: Crystal structure of the Notch Dimer complex on Hes1 SPS. The Notch complex dimers assembled on the Hes1 SPS. CSL bound to NREs 2 and 4 is depicted with light- and dark-green ribbons; red and pink ribbons depict the N-terminal of MAM; and the ANK domain of the NICD is denoted with light- and dark-blue ribbons. Adapted with permission from Macmillan Publishers Ltd.: Nat. Struct. Mol. Biol. (17), copyright 2010.

This study aims to investigate the Notch pathway in Hes1 and to compare the SPS versus single NREs in terms of protein-DNA binding structure. Results here indicate which NREs in Hes1 are critical for RBPJ-k binding, and attempt to address the question of Notch ternary complex recruitment differences on a single NRE and SPS. RBPJ-k will be further investigated, as this DNA-binding protein allows facilitation of the Notch dimer complex and may be a key target in future treatments. Understanding which NREs in Hes1 are required for structure and function formation may allow us to develop therapies that can elucidate an effect on the essential signaling pathway in the near future.

Experimental Procedures

SupT1 Nuclear Extract Creation

SupT1 cells were obtained from ATCC (Manassas, VA) and grown in culture for two weeks. HyClone RPMI-1640 medium (25mM HEPES, L-Glutamine) supplemented with 10% fetal bovine serum (FBS) and 1% penicillin/streptomycin was used, and cells were grown at 37°C with 5% CO_2. HyClone RPMI-1640 medium was purchased from Fisher Scientific (Pittsburgh, PA).

Cells were grown to a final concentration of 1.32 x 10^6 cells/ml in 4.8 liters. Cells were harvested at 3000 RPM for 15 minutes, and then placed into a hypotonic buffer (10mM Tris-HCl pH 7.9, 10mM NaCl, 1.5mM $MgCl_2$, 2mM DTT, 0.2mM PMSF, 1X protease inhibitor), and Dounce homogenized 30 strokes using a Wheaton B loose pestle. Cell debris were then pelleted, and the homogenate was obtained in hypertonic nuclear extract buffer (NEB 20mM Tris-HCl pH 7.9, 420mM NaCl, 1.5mM $MgCl_2$, 0.2mM EDTA, 25% glycerol, 2mM DTT, 0.2mM PMSF, 1X protease inhibitor) and Dounce homogenized 20 strokes using a Wheaton A tight pestle. Homogenate was then poured into a beaker with a stir bar to remove viscous DNA clot and spun down at 20,000 RPM for 35 minutes. Supernatant was then removed, and SupT1 cell nuclear extract (SupT1 NE) was dialyzed overnight to remove salt impurities in dialysis buffer (20mM Tris-HCl pH 7.9, 50mM KCl, 1.5mM $MgCl_2$, 0.2mM EDTA, 10% glycerol, 1mM DTT, 0.2mM PMSF). SupT1 NE was then quantified via BCA assay for a concentration of 3.3μg/μl, frozen down in liquid nitrogen, and stored at -80°C.

Purified RBPJ-k protein was provided courtesy of Rhett Kovall at the University of Cincinnati, at a concentration of 12μM (670 ng/μl) in buffer (20mM HEPES pH 7.9, 100mM KCl, 10% glycerol, 0.2mM EDTA, 1mM DTT, 0.2mM PMSF). It was then frozen in liquid nitrogen as 25μL aliquots stored at -80°C.

Western Blot of SupT1 Nuclear Extract and Purified RBPJ-k

10% SDS-PAGE gels were run at 200V for approximately 90 minutes to resolve proteins. Transfers were done at 30mAmps overnight at 4°C, and PVDF membrane was blocked in TBS-T/5% (250μl 100% Tween per 500ml TBS) dried milk for 1 hour. Western blots were conducted to identify RBPJ-k using rabbit anti-RBPSUH antibody purchased from Cell Signaling Technology (Danvers, MA). Primary antibody was incubated 1:1000 overnight at 4°C in TBS-T/5%; secondary antibody mouse anti-rabbit HRP conjugate was incubated 1:5000 for an hour at room temperature in TBS-T. HRP substrate was added for one minute, and membrane was imaged via ImageQuant LAS4000 CCD (General Electric) with a chemiluminescence lens exposure for 60 seconds.

Generation of Purified Hes1 Double-Stranded DNA (dsDNA)

Complementary oligonucleotides were purchased from Eurofins Genomics (Louisville, KY). The forward DNA sequences of each oligo used in these studies are listed in Table 1. The reverse sequence is not shown but it is the complement. Oligonucleotides were re-suspended in MilliQ water for a stock concentration of 184μM (3μg/μl). 5μl of each complementary oligonucleotide in MilliQ water was mixed and annealed under the thermal cycler conditions listed in Table 2. Then, 1.7μl (300pmol,

5μg) of the annealed DNA mixture was digested with 50 units of S1 Nuclease from Promega Corp. (Madison, WI) in reaction buffer (50mM sodium acetate, 0.6M NaCl, 4.5mM $ZnSO_4$) for 30 minutes at room temperature to remove any remaining single-stranded DNA (ssDNA). Digest reaction was stopped with 10μl of 0.5M EDTA at 70°C for 10 minutes. The digest was then purified using a PureLink PCR Purification Combo Kit by Invitrogen (Vilnius, LT). The resulting sample, referred to as purified dsDNA, was quantified via NanoDrop to determine the amount of Hes1 dsDNA. Percentage yield after S1 nuclease digestion of ssDNA was about 20-50% (60pmol-150pmol,1μg-2.5μg) dsDNA.

Table 1

Wild-Type and Mutant Promoter Sequences

Hes1 Forward Primer	Primer Sequence (5' – 3')
	(NRE1) (NRE2) (NRE3) (NRE4)
Hes1 WT	ACTGTCGACTC**CTCCCAT**TGGCTGAAAGTTACT**GTGGGAA**AGAAAGT**TTGGGAA**GT**TTCACAC**GAGGATCCAGT
WT(2-4)	ACTGTCGACCT**GTGGGAA**AGAAAGT**TTGGGAA**GT**TTCACAC**GAGGATCCAGT
M2	ACTGTCGACCT**GTCGCAA**AGAAAGT**TTGGGAA**GT**TTCACAC**GAGGATCCAGT
M4	ACTGTCGACCT**GTGGGAA**AGAAAGT**TTGGGAA**GT**TTGAGAC**GAGGATCCAGT
M2/4	ACTGTCGACCT**GTCGCAA**AGAAAGT**TTGGGAA**GT**TTGAGAC**GAGGATCCAGT
MutAB	GGTTACT**GACGCTA**AGAAAGT**TTGGGAA**GT**TAGAGTC**GAGCCGTTCC
Mtall	ACTGTCGACCT**TACGCTA**AGAAAGT**TTAGAAA**GT**TATATTC**GAGGATCCAGT
Mtall2	GACAT**TAAGCTA**AGAAAGT**TTAGAAA**GT**TATATTC**GATCA
NRE2	CGGCCT**GTGGGAA**ACTTCC
NRE2m	GGCCT**GTCGCAA**ACTTCC
NRE3	CGGCC**TTGGGAA**CTTCC
NRE3m	CGGCC**TTCGCAA**CTTCC
NRE4	CGGCCT**TTCACAC**ACTTCC
NRE4m	CGGCCT**TTGAGAC**ACTTCC
SPS	CGGCCT**GTGGGA**AAGAAAGTTATACAAGT**TTCACAC**ACTTCC
SPSm	CGGCCT**GTCGCA**AAGAAAGTTATACAAGT**TTCACAC**ACTTCC
(other primers)	
NFKB	AGTTGAGGGGACTTTCCCAGGC
GATA	GCAGTTAACTGATAATGACACTGTG

Notes: NRE binding sites are denoted in blue.
Underline = mutation from Wild Type (WT)
Restriction digest DNA ends = 5'- ACTGTCGAC, GATCCAGT -3'
Nam et al., (2007) DNA ends = 5'- GGTTA, CCGTTCC -3'
Friedmann & Kovall, (2010) DNA ends = 5'- CGGCC, ACTTCC -3'

Table 2
Thermal Cycler Conditions for Generation of Hes1 dsDNA

Segment	Cycles	Temperature (°C)	Time
1	1	95	5 min
2	1	85	30 sec
3	1	75	30 sec
4	1	65	30 sec
5	1	55	30 sec
6	1	45	30 sec
7	1	4	2 min

Electrophoretic Mobility Shift Assay (EMSA)

EMSAs were performed with polyacrylamide gel electrophoresis (PAGE), prepared with 37.5:1 ratio of acrylamide to bis-acrylamide as shown in Table 3, with 0.5X TBE (0.045M tris base, 0.045M boric acid, 0.001M EDTA) running buffer. The DNA-protein binding reaction final volume was 20µl. The final concentrations of dsDNA, SupT1 NE, and purified RBPJ-k were as follows: 400nM (8-35pmol, 140ng-600ng) dsDNA; 10-30µg of SupT1 NE; and 600nM (672ng) RBPJ-k in 1X gel shift buffer (GSB 20mM Tris-HCl pH 7.9, 50mM KCl, 5mM $MgCl_2$, 10% glycerol, 5mM DTT, 0.06mg/ml BSA) +/- 0.1-2µg LightShift Poly(dI-dC) from Thermo Scientific (Lithuania). Tubes were kept on ice for 20 minutes. A 20µl sample was loaded in the PAGE gel matrix along with 140ng Ultra Low Range DNA Ladder from Invitrogen (Vilnius, LT), run at 180V for 75

minutes. Gels were stained in 0.5X TBE, supplemented with 1X SYBR Gold nucleic acid gel stain from Invitrogen (Eugene, OR) for 25 minutes, and immediately visualized via ImageQuant LAS4000 CCD (General Electric) with a blue-light lens exposure for ½ - 3 seconds.

Table 3
Preparation of 10ml Polyacrylamide Gel Mixture for One 8×8 cm Gel

PAGE %	6%	10%
40% Acrylamide (37.5:1; C = 2.7)	1.5ml	2.5ml
10X TBE (0.5X final)	0.5ml	0.5ml
Nanopure H_20	8ml	7ml
10% APS	100µl	100µl
TEMED	10µl	10µl

Results

Identification of RBPJ-k

Below is a western blot of the SupT1 cell nuclear extract (SupT1 NE) and purified murine RBPJ-k (Figure 6). RBPSUH antibody is specific for human, mouse, rat, and monkey CSL protein. Results indicate that SupT1 NE and purified murine protein contains CSL protein RBPJ-k. SupT1 NE contains the native-size protein and appears around expected molecular weight of 61kDa (Xu et al., 2017). Lower molecular weight of purified RBPJ-k is attributed to the recombinant protein size.

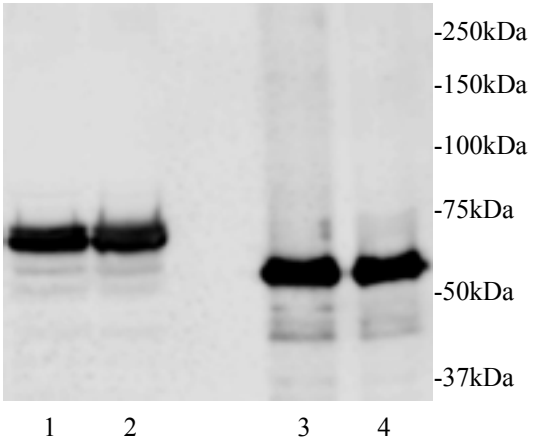

Figure 6: Western blot of SupT1 NE and purified RBPJ-k.
10% SDS-PAGE with a primary antibody against RBPJ-k. Lanes 1 and 2 contain 60μg and 100μg of SupT1 NE respectively. Lanes 3 and 4 contain 134ng and 67ng of purified RBPJ-k, respectively. The protein ladder is not shown, but is depicted by the indicated labels.

Hes1 SPS Interactions with SupT1 NE

In order to visualize the Notch complex binding Hes1 dsDNA, an electrophoretic mobility shift assay of unpurified Hes1 WT dsDNA incubated with SupT1 NE was conducted (Figure 7). The dsDNA was not digested to remove ssDNA. PolydI-dC was not used. Although SupT1 NE is interacting with free probe DNA, no clear shift bands are produced to visually specify Notch complex.

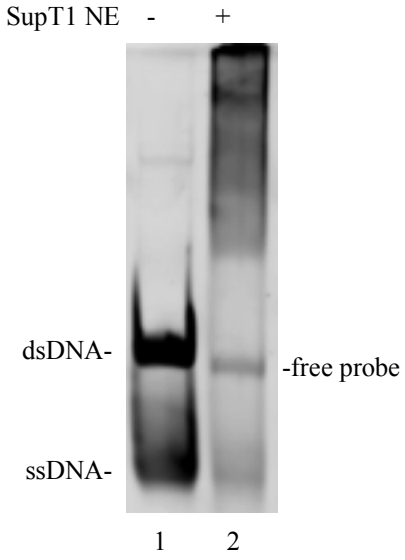

WT(2–4) – ACTGTCGACCTGTGGGAAAGAAAGTTTGGGAAGTTTCACACGAGGATCCAGT

Figure 7: EMSA of SupT1 NE with Hes1 WT dsDNA.
10% PAGE EMSA of SupT1 NE binding to unpurified 600ng Hes1 WT (2-4) dsDNA. Lane 1 contains free probe WT dsDNA, and Lane 2 contains WT dsDNA incubated with 30µg of SupT1 NE. DNA sequence is shown below the figure.

S1 Nuclease Digest of Unpurified Hes1 dsDNA

To remove the ssDNA left over from the annealing process, an S1 digest was performed on the unpurified Hes1 WT dsDNA (Figure 8). After the S1 digest and

subsequent purification, the ssDNA from Lane 1 is removed from the purified dsDNA in Lane 2. The dsDNA migrates near the expected molecular weight of 50bp.

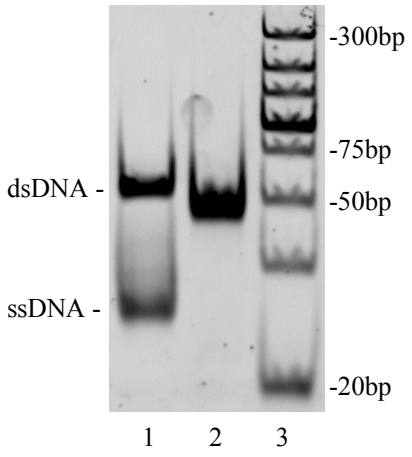

WT(2–4) – ACTGTCGACCTGTGGGAAAGAAAGTTTGGGAAGTTTCACACGAGGATCCAGT

Figure 8: EMSA of unpurified and purified Hes1 WT dsDNA.
10% PAGE EMSA that compares 140ng of unpurified and purified Hes1 WT (2-4) dsDNA. Lane 1 contains unpurified dsDNA, and Lane 2 contains purified dsDNA. Lane 3 contains 140ng of dsDNA ladder depicted by the indicated labels. DNA sequence is shown below the figure.

Purified Hes1 SPS and Mutant Interactions with SupT1 NE

Upon digestion of ssDNA, the newly purified dsDNA was again incubated with SupT1 NE to determine whether clear shift bands can now be visualized (Figure 9). As expected, the WT dsDNAs migrate at 50-75bp, and the mutants migrate around 50bp. SupT1 NE is again shifting most the free probe WT dsDNA, and no clear shift bands can be visualized. Surprisingly, SupT1 NE is also shifting the SPS mutants.

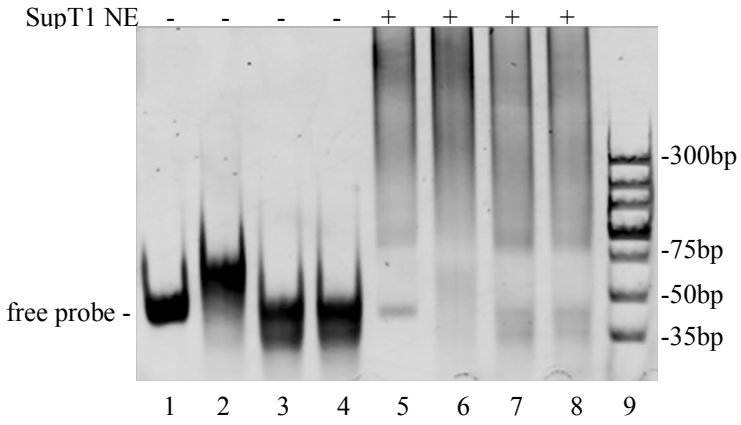


```
WT(2-4) –                        ACTGTCGACCTGTGGGAAAGAAAGTTTGGGAAGTTTCACACGAGGATCCAGT
Hes1 WT – ACTGTCGACTCCTCCCATTGGCTGAAAGTTACTGTGGGAAAGAAAGTTTGGGAAGTTTCACACGAGGATCCAGT
M2 –                             ACTGTCGACCTGTCGCAAAGAAAGTTTGGGAAGTTTCACACGAGGATCCAGT
M4 –                             ACTGTCGACCTGTGGGAAAGAAAGTTTGGGAAGTTTGAGACGAGGATCCAGT
```

Figure 9: EMSA of SupT1 NE with purified Hes1 WT and mutant dsDNA. 10% PAGE EMSA of SupT1 NE binding to 140ng purified Hes1 WT and mutant dsDNA. Lanes 1, 2, 3, and 4 contain free probe WT (2-4), Hes1 WT, M2 and M4 dsDNA, respectively. Lanes 5, 6, 7, and 8 contain WT (2-4), Hes1 WT, M2, and M4 dsDNA, respectively, incubated with 2.3µg of SupT1 NE. Lane 9 contains 140ng of dsDNA ladder depicted by the indicated labels. DNA sequences are shown below the figure.

EMSA Optimization with PolydI-dC, Gel %, and Cross-Linking

To optimize with a non-specific competitor, polydI-dC was added to these EMSAs (Figure 10). Lower-percentage acrylamide gels were also tested, along with a higher cross-linking ratio to allow for increased pore sizes. Purified Hes1 WT dsDNA is again incubated with SupT1 NE; however, in the presence of non-specific competitor polydI-dC. The WT dsDNA migrates around 50bp, as expected.

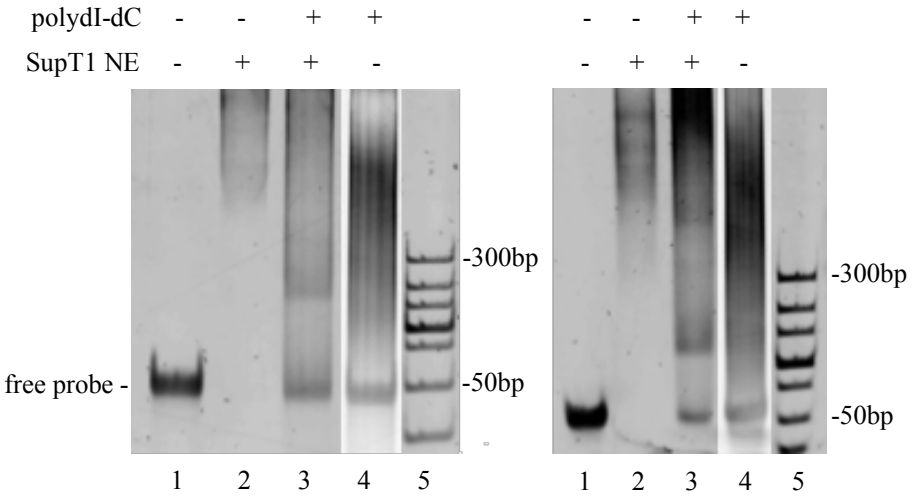

WT(2–4) – ACTGTCGACCTGTGGGAAAGAAAGTTTGGGAAGTTTCACACGAGGATCCAGT

Figure 10: EMSA of SupT1 NE and Hes1 WT dsDNA with polydI-dC.
10% (left) and 4% (right) PAGE EMSA (61.5:1) of SupT1 NE binding to 140ng purified Hes1 WT (2-4) dsDNA. Lane 1 contains free probe WT dsDNA. Lanes 2 and 3 contain WT dsDNA, respectively, incubated with 10µg of SupT1 NE, with and without 2µg of polydI-dC. Lane 4 contains WT dsDNA and 2µg of polydI-dC (smearing) for background measure and has been adjusted for intensity. Lane 5 contains 140ng of dsDNA ladder depicted by the indicated labels. DNA sequence is shown below the figure.

PolydI-dC was added to Lanes 3 and 4. In Lane 2, SupT1 NE is interacting with free probe dsDNA. When adding polydI-dC in Lane 3, there is an increased amount of free probe DNA, which may suggest some non-specific binding. The gel on the right is a lower % acrylamide, and both gels have increased pore sizes. However, even under these conditions with the reduction of non-specific binding, clear shift bands still cannot be visualized.

NFKB and GATA Interactions with SupT1 NE

To test the SupT1 NE for control transcription factors that can be identified with clear shift bands, the following EMSA was conducted to visualize unpurified NFKB and GATA dsDNA incubated with SupT1 NE (Figure 11). NFKB and GATA dsDNA were not digested to remove ssDNA, and polydI-dC was not used. SupT1 NE is interacting with free probe dsDNA in both instances. Clear shift bands are produced that visualize NFKB and GATA complexes bound to dsDNA.

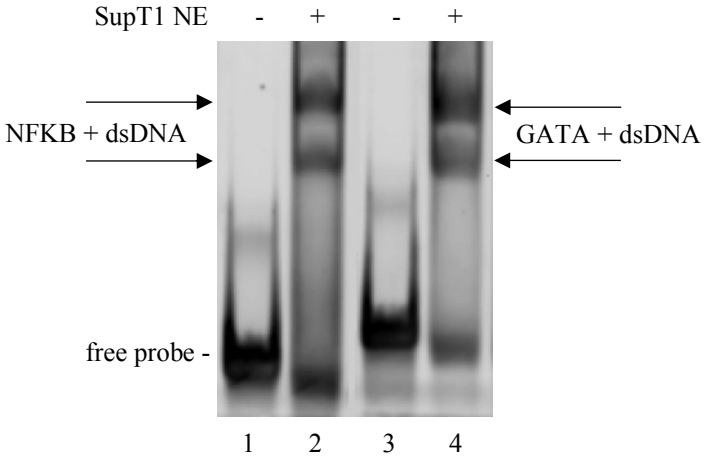

NFKB –AGTTGAGGGGACTTTCCCAGGC

GATA – GCAGTTAACTGATAATGACACTGTG

Figure 11: EMSA of SupT1 NE and NFKB/GATA dsDNA.
10% PAGE EMSA of SupT1 NE binding to 600ng unpurified NFKB dsDNA. Lanes 1 and 3 contain free unbound NFKB and GATA dsDNA respectively. Lanes 2 and 4 contain NFKB and GATA dsDNA, respectively, incubated with 30µg of SupT1 NE. The protein-DNA complexes are depicted by the arrows. DNA sequences are shown below the figure.

Hes1 SPS ssDNA Interactions with RBPJ-k

The following EMSAs examine the binding effects of RBPJ-k on the Hes1 SPS with ssDNA and dsDNA (Figure 12). In this EMSA, purified murine RBPJ-k protein is incubated with unpurified WT ssDNA and dsDNA. PolydI-dC was not used.

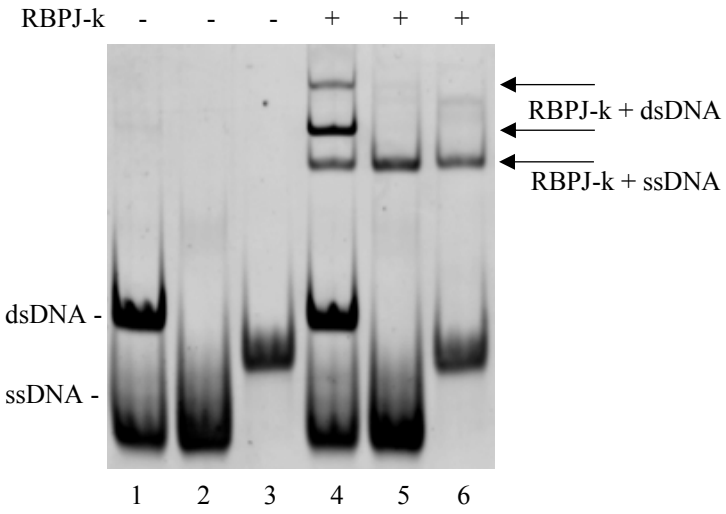

WT(2–4) – ACTGTCGACCT**GTGGGAA**AGAAAGT**TTGGGAA**GT**TTCACAC**GAGGATCCAGT

Figure 12: EMSA of RBPJ-k with Hes1 WT ssDNA and dsDNA.
10% EMSA of purified RBPJ-k binding to 400nM unpurified Hes1 WT (2-4) dsDNA and ssDNA. Lanes 1, 2, and 3 contain free probe WT dsDNA, ssDNA forward primer, and ssDNA reverse primer, respectively. Lanes 4, 5, and 6 contain WT dsDNA, ssDNA forward primer, and ssDNA reverse primer, respectively, incubated with 600nM RBPJ-k. Lane 6 contains 140ng dsDNA ladder depicted by the indicated labels. The protein-DNA complexes are depicted by the arrows. DNA sequence is shown below the figure.

The purified RBPJ-k protein is interacting with both the dsDNA and ssDNA. Clear shift bands are produced that appear to relate to three RBPJ-k complexes bound to WT dsDNA in Lane 5. RBPJ-k is also interacting with the WT ssDNA, producing one shift

band when bound to the ssDNA. It is suspected the three shift bands that are produced by RBPJ-k binding to the unpurified WT dsDNA are a result of RBPJ-k interacting with leftover ssDNA.

Purified Hes1 SPS Interactions with RBPJ-k

To investigate the three shift bands formed when RBPJ-k is incubated with unpurified WT dsDNA, the dsDNA was digested to remove any remaining ssDNA (Figure 13). In this EMSA, purified murine RBPJ-k protein is incubated with purified WT Hes1 dsDNA. PolydI-dC was not used.

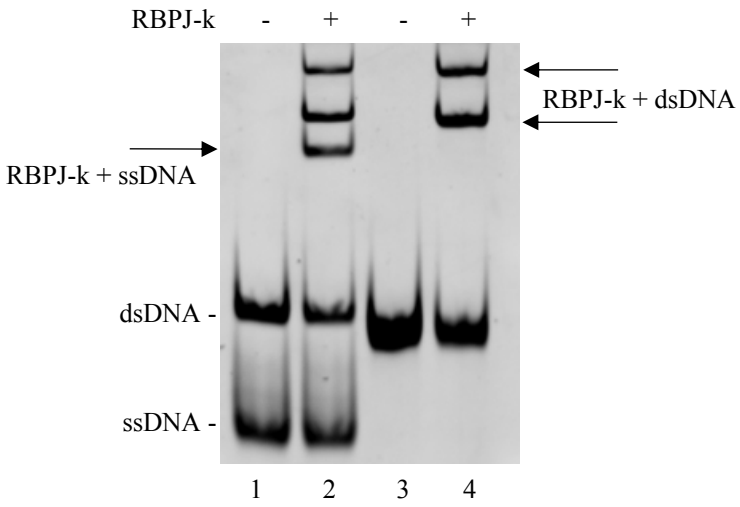

WT(2–4) – ACTGTCGACCTGTGGGAAAGAAAGTTTGGGAAGTTTCACACGAGGATCCAGT

Figure 13: EMSA of RBPJ-k with Hes1 WT ssDNA and dsDNA.
10% EMSA of purified RBPJ-k binding to 400nM unpurified and purified Hes1 WT (2-4) dsDNA. Lanes 1 and 2 contain unpurified and purified free probe WT dsDNA, respectively. Lanes 3 and 4 contain unpurified and purified WT dsDNA, respectively, incubated with 600nM RBPJ-k. The protein-DNA complexes are depicted by the arrows. DNA sequence is shown below the figure.

One of the shift bands produced by RBPJ-k binding to the unpurified WT dsDNA in Lane 2 is removed upon digestion of the ssDNA, with RBPJ-k binding to the purified WT dsDNA in Lane 4. Clear shift bands are produced that visualize two RBPJ-k complexes bound to the purified WT dsDNA.

Hes1 SPS and Mutant Interactions with RBPJ-k

After removal of ssDNA, the following EMSA was conducted to examine the binding effects of RBPJ-k on the Hes1 SPS (Figure 14). In order to asses which NRE site mutants affect RBPJ-k binding, purified RBPJ-k is incubated with single site mutants M2 and M4. To test binding of other sites, WT dsDNA was also tested with all the NRE sites (1-4). PolydI-dC was not used. The WT (NRE 2-4) and mutants M2 and M4 migrate around the expected molecular weight of 50bp. The WT (NRE 1-4) also migrates around the expected molecular weight of 75bp. The purified RBPJ-k protein is interacting with both the WT dsDNA variants. Clear shift bands are produced that visualize two RBPJ-k complexes bound to both WT dsDNAs. RBPJ-k is also interacting with mutants M2 and M4 dsDNA. The upper protein-DNA shift band is seen with the WT dsDNA and the mutants. Mutants in Lanes 4 and 6 show similar binding structures to those in the WT Lanes 2 and 8, and thus are not sufficient to make a visual comparison of binding differences.

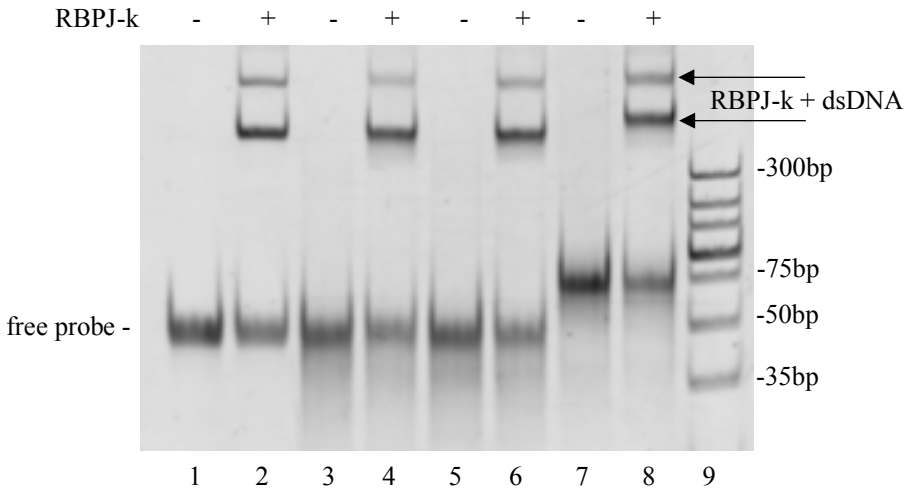


```
WT(2-4) –                          ACTGTCGACCTGTGGGAAAGAAAGTTTGGGAAGTTTCACACGAGGATCCAGT
M2 –                               ACTGTCGACCTGTCGCAAAGAAAGTTTGGGAAGTTTCACACGAGGATCCAGT
M4 –                               ACTGTCGACCTGTGGGAAAGAAAGTTTGGGAAGTTTGAGACGAGGATCCAGT
Hes1 WT – ACTGTCGACTCCTCCCATTGGCTGAAAGTTACTGTGGGAAAGAAAGTTTGGGAAGTTTCACACGAGGATCCAGT
```

Figure 14: EMSA of RBPJ-k with Hes1 WT and mutant WT dsDNA.
10% EMSA of purified RBPJ-k binding to 400nM purified Hes1 WT and mutant dsDNA. Lanes 1, 3, 5, and 7 contain free probe WT (2-4), M2, M4, and Hes1 WT dsDNA, respectively. Lanes 2, 4, 6, and 8 contain WT (2-4), M2, M4, and Hes1 WT dsDNA, respectively, incubated with 600nM RBPJ-k. Lane 9 contains 140ng dsDNA ladder depicted by the indicated labels. The protein-DNA complexes are depicted by the arrows. DNA sequences are shown below the figure.

Hes1 SPS and Alternative Mutant Interactions with RBPJ-k

This subsequent EMSA investigates purified RBPJ-k binding purified WT and other mutant variants (Figure 15). Mutants used in the EMSA are site 2 and 4 NRE mutants (M2/4), and all site NRE mutants (Mtall). PolydI-dC was not used. Again, the WT and mutant variants migrate around the expected molecular weight of 50bp. The purified RBPJ-k protein is interacting with the WT and producing clear shift bands that visualize two RBPJ-k complexes bound to WT dsDNA. RBPJ-k is also interacting with both

mutant dsDNA variants. Eliminating both RBPJ-k binding sites still seems to produce both protein-DNA shift bands (Lane 4), as seen with previous mutant dsDNA. The upper protein-DNA band in Lanes 4 and 6 are similar in structure to the WT; a visual difference cannot be identified.

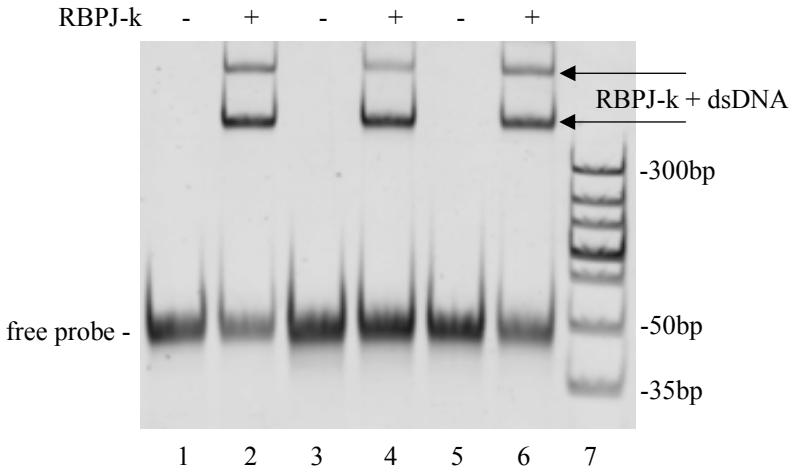


```
WT(2-4) –       ACTGTCGACCTGTGGGAAAGAAAGTTTGGGAAGTTTCACACGAGGATCCAGT
M2/4 –          ACTGTCGACCTGTCGCAAAGAAAGTTTGGGAAGTTTGAGACGAGGATCCAGT
Mtall –         ACTGTCGACCTTACGCTAAGAAAGTTTAGAAAGTTATATTCGAGGATCCAGT
```

Figure 15: EMSA of RBPJ-k with Hes1 WT, M2/4, and Mtall dsDNA.
10% EMSA of purified RBPJ-k binding to 400nM purified Hes1 WT (2-4), M2/4, and MTall, dsDNA. Lanes 1, 3, and 5 contain free probe WT, M2/4, and Mtall dsDNA, respectively. Lanes 2, 4, and 6 contain WT, M2/4, and MTall dsDNA respectively, incubated with 600nM RBPJ-k. Lane 7 contains 140ng dsDNA ladder depicted by the indicated labels. The protein-DNA complexes are depicted by the arrows. DNA sequences are shown below the figure.

PolydI-dC Effects on Hes1 SPS and Mutant Interactions with Titrated RBPJ-k

The purpose of this gel is to test Hes1 dsDNA variants with titrating amounts of RBPJ-k to adjust for K_D differences (Figure 16). PolydI-dC was also added to in inhibit non-specific binding. The mutant dsDNA used in this EMSA (MutAB) has a sequence and 5' to 3' ends that are identical to the site 2/ 4 NRE mutant, which did not shift RBPJ-k in previously published research (Nam et al., 2007). Both the WT and MutAB dsDNA variants migrate around the expected molecular weight of 50bp. As before, the purified RBPJ-k protein is producing clear shift bands when interacting with the WT dsDNA, causing two different molecular weight protein-DNA complexes. This is similar to the two complexes seen in the previous EMSAs.

RBPJ-k still seems to be interacting with the new MutAB dsDNA, even when the protein is titrated from left to right. Although the upper shift band of the mutant in Lane 7 does not seem as intense as the WT in Lane 2, the shift bands have similar structure when comparing titrated WT (Lanes 3-5) to titrated MutAB (Lanes 8-10). As a result, a visual difference is difficult to conclude with the "smearing" polydI-dC background. Titration of the purified protein with MutAB did not produce a significant visual difference from the WT. This EMSA method may not have enough sensitivity, and other EMSA methods might allow for a higher sensitivity. If there is any difference, a quantification may reveal this.

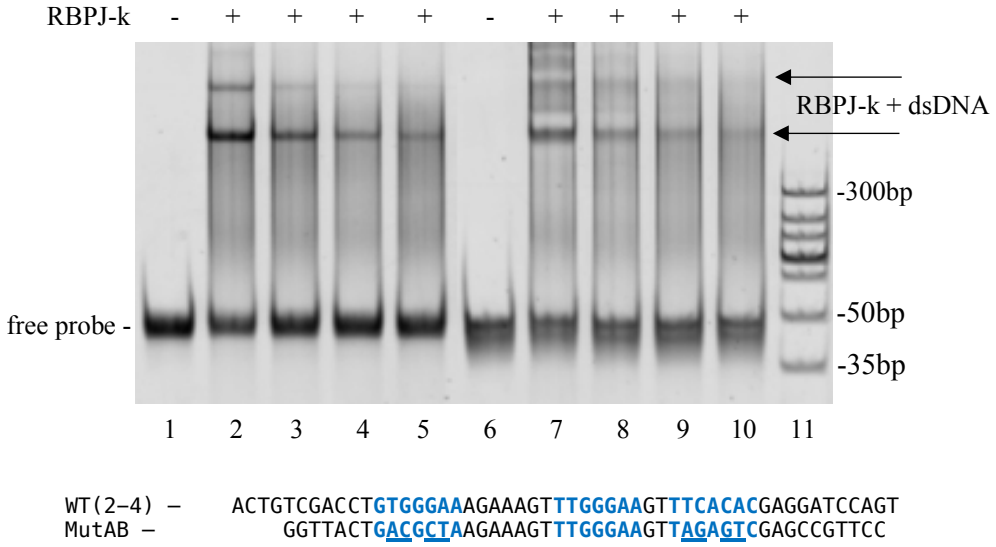

Figure 16: EMSA titration of RBPJ-k with Hes1 WT and MutAB dsDNA. 10% EMSA of purified RBPJ-k binding to 400nM purified Hes1 WT (2-4) (left) and MutAB (right) dsDNA. Lanes 1 and 6 contain free probe WT and MutAB dsDNA, respectively. Lanes 2-5 (WT) and 7-10 (MutAB) contain dsDNA incubated with 600, 300, 150, 80nM RBPJ-k, respectively, and 100ng of polydI-dC (smearing). Lane 11 contains 140ng dsDNA ladder depicted by the indicated labels. The protein-DNA complexes are depicted by the arrows. DNA sequences are shown below the figure.

PolydI-dC Effects on Hes1 Alternative Mutant Interactions with RBPJ-k

To test the alternative mutants that have all NRE sites removed in presence of polydI-dC, Mtall and Mtall2 were incubated with RBPJ-k. Mtall is a repeat of all NRE site mutants, and Mtall2 has the restriction digest overhangs from Mtall removed. MutAB was tested again for comparison. Mtall2 migrates around the molecular weight of 35bp; Mtall and MutAB migrate near the expected molecular weight of 50bp, all as expected. The purified RBPJ-k protein is interacting with the alternative mutants, and clear shift bands are produced that visualize two RBPJ-k complexes bound to mutant dsDNA, even

in the presence of polydI-dC. The polydI-dC background may be covering up the upper shift band, but all mutants seem to have similar binding structure, even when completely destructing the DNA. With polydI-dC, the upper and lower protein-DNA bands in Lanes 2, 4, and 6 appear to be less intense than previous gels without the non–specific competitor. However, visual comparisons cannot be made without methods of quantification.

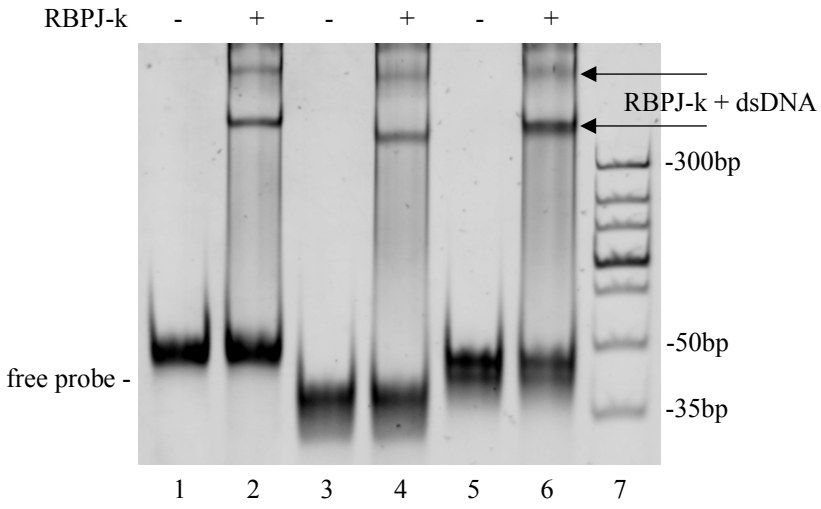


```
Mtall–          ACTGTCGACCTTACGCTAAGAAAGTTTAGAAAGTTATATTCGAGGATCCAGT
Mtall2 –              GACATTAAGCTAAGAAAGTTTAGAAAGTTATATTCGATCA
MutAB –             GGTTACTGACGCTAAGAAAGTTTGGGAAGTTAGAGTCGAGCCGTTCC
```

Figure 17: EMSA of RBPJ-k with Hes1 MTall, MTall2, and MutAB dsDNA with polydI-dC. 10% PAGE EMSA of purified RBPJ-k binding to 400nM purified Hes1 mutants; MTall, MTall2, and MutAB dsDNA. Lanes 1, 3, and 5 contain free probe MTall, MTall2, and MutAB dsDNA, respectively. Lanes 2, 4, and 6 contain MTall, MTall2, and MutAB dsDNA, respectively, incubated with 600nM RBPJ-k and 100ng of polydI-dC (smearing). Lane 7 contains 140ng dsDNA ladder depicted by the indicated labels. The protein-DNA complexes are depicted by the arrows. DNA sequences are shown below the figure.

High Salt Effects on Hes1 Mutant Interactions with RBPJ-k

Previous research has shown that the binding affinity of RBPJ-k to Hes1 dsDNA is decreased in presence of high salt (Friedmann & Kovall, 2010). To test the effect of high salt concentration on the binding of RBPJ-k to the mutant dsDNA presented in these studies, MutAB was incubated with RBPJ-k and increasing amounts of NaCl. The MutAB dsDNA migrates near the expected molecular weight of 50bp.

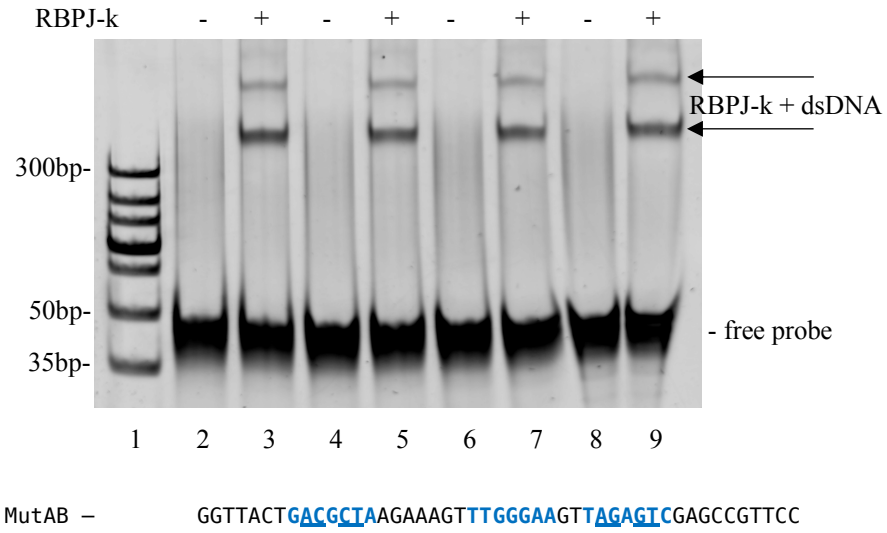

Figure 18: EMSA of RBPJ-k and MutAB dsDNA in presence of high salt.
10% EMSA of purified RBPJ-k binding to 400nM purified MutAB dsDNA. Lanes 2, 4, 6 and 8 contain free probe MutAB dsDNA and 0, 100, 200, and 450mM NaCl, respectively, with 100ng polydI-dC (smearing) and 0.1% NP-40. Lanes 3, 5, 7 and 9 contain MutAB dsDNA and 0, 100, 200, and 450mM NaCl, respectively, with 600nM RBPJ-k and 100ng of polydI-dC (smearing), 0.1% NP-40. Lane 1 contains 140ng dsDNA ladder depicted by the indicated labels. The protein-DNA complexes are depicted by the arrows. DNA sequence is shown below the figure.

When adding increasing amounts of salt (left to right), both the shift bands are still present. Even in the presence of polydI-dC, adding higher amounts of salt does not seem

to change the binding seen. NP-40 is also added to reduce the "smearing" background seen at the top of the lanes. At the higher amounts of salt (Lanes 7 and 9), the shift bands should be diminished, as suggested by previous research. As a result, no visual difference is seen in any of the lanes, although the higher salt amounts appear to skew the dsDNA.

Alternative Hes1 SPS Interactions with RBPJ-k

To investigate whether changing the DNA 5' to 3' ends will affect binding, the same Hes1 SPS DNA ends that were used in the thermodynamic studies of RBPJ-k binding (Friedmann & Kovall, 2010) were used in this EMSA (Figure 19). SPS and SPSm dsDNA variants were incubated with RBPJ-k in presence of polydI-dC and NP-40. SPS and SPSm dsDNA are sized as expected. SPS dsDNA produces two shift bands relating to the two different RBPJ-K + dsDNA molecular weight complexes. SPSm, with a mutation in NRE 2, also produces two shift bands; it does not have a visual difference in comparison to SPS dsDNA and is not different without means of quantification. This may suggest that the cause of mutant binding to dsDNA seen in this study is a result of something other than the ends that flank the dsDNA.

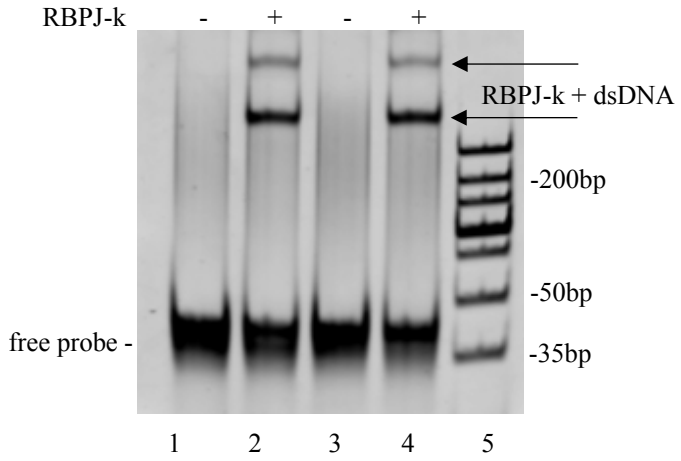

SPS – CGGCCTGTGGGAAAGAAAGTTATACAAGTTTCACACACTTCC
SPSm – CGGCCTGTCGCAAAGAAAGTTATACAAGTTTCACACACTTCC

Figure 19: EMSA of RBPJ-k with SPS and SPSm dsDNA.
10% EMSA of purified RBPJ-k binding to 400nM purified single site combination SPS dsDNA, and single site combination mutant SPSm. Lanes 1 and 3 contain free unbound SPS and SPSm dsDNA, respectively. Lanes 2 and 4 contain SPS and SPSm dsDNA respectively, incubated with 0.6μM RBPJ-k. Lanes 1-4 contain 100ng of polydI-dC (smearing) and 0.1% NP-40. Lane 5 contains 140ng dsDNA ladder depicted by the indicated labels. The protein-DNA complexes are depicted by the arrows. DNA sequences are shown below the figure.

Alternative DNA Interactions with RBPJ-k

To test binding to other dsDNA sequences not related to the Hes1 promoter, NFKB and GATA sequences were examined for RBPJ-k binding. In this EMSA, RBPJ-k was incubated with NFKB and GATA dsDNA (Figure 20). PolydI-dC was also included. Both NFKB and GATA dsDNA migrate between the expected molecular weights of 20-35bp.

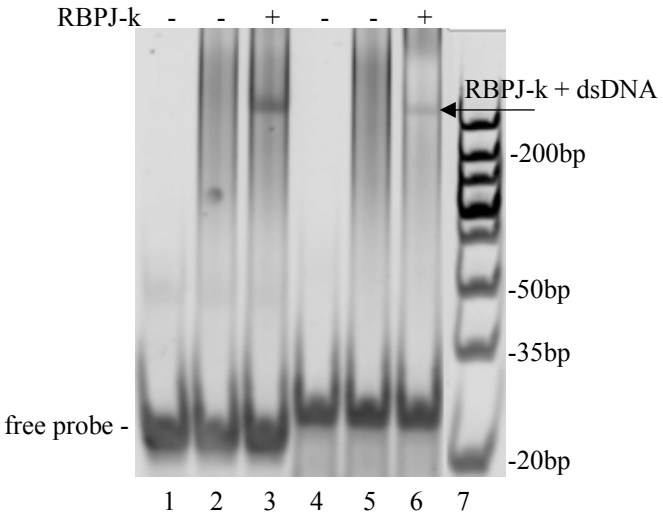

NFKB –AGTTGAGGGGACTTTCCCAGGC

GATA – GCAGTTAACTGATAATGACACTGTG

Figure 20: EMSA of RBPJ-k with NFKB and GATA dsDNA.
10% EMSA of purified RBPJ-k binding to 400nM unpurified GATA and NFKB dsDNA. Lanes 1 and 4 contain free probe GATA and NFKB dsDNA, respectively. Lanes 2 and 5 contain free probe GATA and NFKB dsDNA, respectively, with 100ng of polydI-dC (smearing). Lanes 3 and 6 contain GATA and NFKB dsDNA respectively, incubated with 0.6μM RBPJ-k and 100ng of polydI-dC (smearing). Lane 7 contains 140ng dsDNA ladder depicted by the indicated labels. The protein-DNA complexes are depicted by the arrows. DNA sequences are shown below the figure.

When RBPJ-k is added to free probe NFKB dsDNA, a shift band can be seen in Lane 3. When RBPJ-k is added to free probe GATA dsDNA, a weaker shift band can be seen in Lane 6. These sequences do not contain any RBPJ-k binding motifs and theoretically should not be shifting the dsDNA, especially in the presence of non-specific inhibitor polydI-dC.

Hes1 NRE 2 and 4 Single Site Interactions with RBPJ-k

To determine if single site NREs on shorter dsDNA would produce visually different shift bands, single site dsDNA was used in presence of polydI-dC and also NP-40 to ensure specific binding. These single sites correspond to the same DNA sequence used in previous thermodynamic studies of RBPJ-k binding (Friedmann & Kovall, 2010). In this EMSA, RBPK-k is incubated with single site Hes1 NRE2; NRE4; and mutants NRE2m and NRE4m (Figure 21). The WT and mutant dsDNA variants migrate near the expected molecular weight of 20bp. RBPJ-k is interacting with NRE2 and NRE4 dsDNA in Lanes 2 and 4, respectively. This interaction seems to produce a more stable visualized shift band than what is seen with internal guanine mutants NRE2m and NRE4m in Lanes 6 and 8, respectively. When comparing wild-type sequences to mutants, Lane 2 to Lane 6, and Lane 4 to Lane 8, a visual difference can be distinguished. The band in the mutant dsDNA variant is far less intense and thus far less stable, suggesting a disruption in binding. The lower RBPJ-k + dsDNA WT shift band is conserved, representing the single binding site seen in previous EMSA figures. The second upper RBPJ-k + dsDNA complex is not seen with the shorter DNA. However, one must note the minimal amounts of binding structures are seen with the mutant dsDNAs, and this may relate to the robust RBPJ-k interactions that were seen in all previous EMSAs.

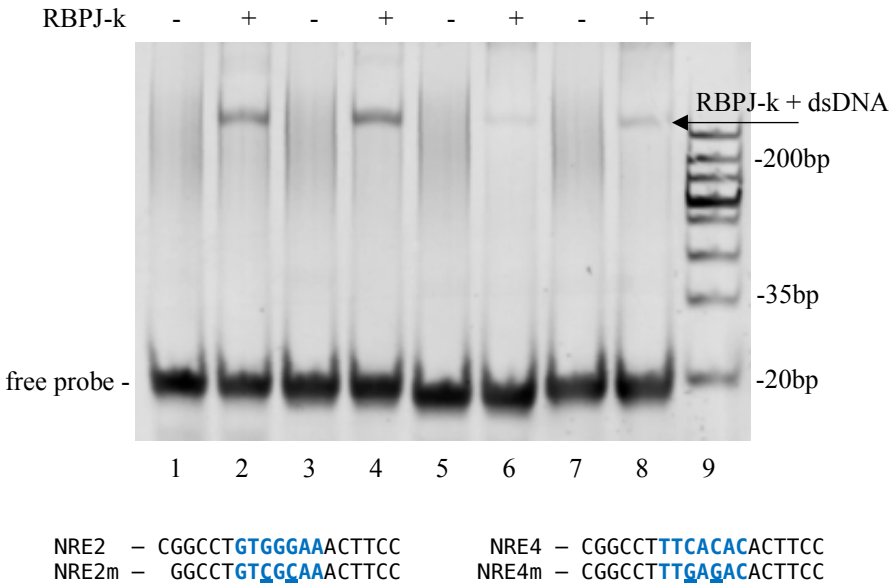

Figure 21: EMSA of RBPJ-k and single site Hes1 NRE2, NRE4, NRE2m, and NRE4m dsDNA. 10% EMSA of purified RBPJ-k binding to 400nM annealed Hes1 single site NRE2, NRE4 dsDNA, and single site mutants NRE2m and NRE4m dsDNA. Lanes 1, 3, 5, and 7 contain free unbound NRE2, NRE4, NRE2m, and NRE4m dsDNA, respectively. Lanes 2, 4, 6, and 8 contain NRE2, NRE4, NRE2m, and NRE4m dsDNA, respectively, incubated with 0.6μM RBPJ-k. Lanes 1-8 contain 100ng of polydI-dC (smearing) and 0.1% NP-40. Lane 9 contains 140ng dsDNA ladder depicted by the indicated labels. The protein-DNA complex is depicted by the arrow. DNA sequences are shown below the figure.

Hes1 NRE 3 Single Site Interactions with RBPJ-k

Since the single site NRE dsDNA variants produced a visually significant difference in Figure 21, this EMSA was conducted to address the functionality questioned through other NREs not in the SPS. RBPK-k is incubated with single site Hes1 NRE3, again in the presence of polydI-dC and NP-40 (Figure 22). WT and mutant dsDNA variants migrate near the expected molecular weight of 20bp. RBPJ-k is interacting with NRE3 dsDNA in Lane 2. When compared to the mutant NRE3m in Lane 4, the protein-DNA

shift band produced in Lane 2 is more intense and thus stable; a visual difference can be distinguished. This shows binding activity through NRE3, and again suggests when the internal guanines are mutated in the NRE, binding structure is lost. Again, the lower shift band is produced, representing a single binding site. This binding structure and visual differences are similar to those seen in the other single site, NRE EMSAs (Figure 21). Likewise, a basal amount of binding structure may be seen through the mutant.

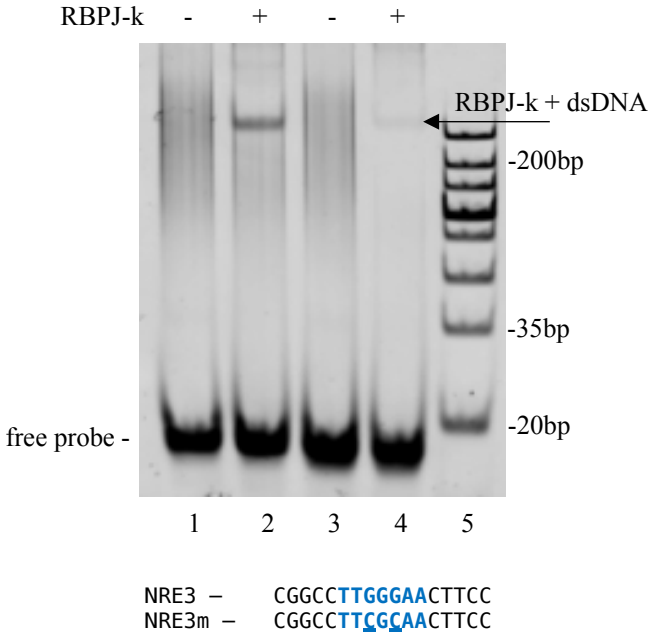

Figure 22: EMSA of RBPJ-k and single site Hes1 NRE3, and NRE3m dsDNA. 10% EMSA of purified RBPJ-k binding to 400nM of annealed Hes1 single site NRE3 dsDNA, and single site mutant NRE3m. Lanes 1 and 3 contain free unbound NRE3 and NRE3m dsDNA, respectively. Lanes 2 and 4 contain NRE3 and NRE3m dsDNA, respectively, incubated with 0.6μM RBPJ-k. Lanes 1-4 contain 100ng of polydI-dC (smearing) and 0.1% NP-40. Lane 5 contains 140ng dsDNA ladder depicted by the indicated labels. The protein-DNA complex is depicted by the arrow. DNA sequences are shown below the figure.

Discussion

An attempt to resolve the structural difference in Notch complex formation on the SPS as opposed to a single NRE was presented in these studies. We confirmed that the SupT1 nuclear extract contained RBPJ-k (Figure 6); previous papers have also shown that this cell nuclear extract contains high amounts of Notch (Yatim et al., 2012). Therefore, this cell nuclear extract would be adequate for our experiments. The SupT1 nuclear extract was first tested for binding to unpurified WT dsDNA (Figure 7). EMSAs showed that although there is a massive shift of free probe, no distinct shift bands are produced to identify protein-DNA complexes from the large smear. Even under optimized conditions, such as the removal of ssDNA (Figures 8, 9), no distinct shift bands were produced. The smear produced by the shift of free probe indicates binding of nuclear extract. However, it is very difficult to conduct an analysis that compares SPS to single NREs when there are no visually distinct shift bands. Adding another NRE site did not have an effect, and surprisingly, all mutant dsDNA is also shifting. This may suggest that there are other factors in the SupT1 nuclear extract possibly interacting with the dsDNA.

Furthermore, the Notch complex is likely too large to be resolved on higher-percentage acrylamide gels with small pores. Even with further optimization using polydI-dC, proper resolution was not achieved to visualize shift bands that relate to the Notch complex binding on Hes1 dsDNA (Figure 10). Increasing the gel pore size did not seem to have an effect either. Although no clear binding structure was resolved from the SupT1 nuclear extract binding to the Hes1 promoter, the amount of free unbound probe is

significantly less in Lane 2 when compared to Lane 3 (Figure 10). This suggests that polydI-dC is added in a sufficient amount to inhibit some non-specific interactions.

Results confirmed positive binding to other transcription factors such as NFKB and GATA by clear resolved shift bands (Figure 11). These resolved protein-DNA shift bands are not seen with Hes1 dsDNA. The technique employed in these EMSAs is sufficient to produce resolved shift bands, as shown by the SupT1 nuclear extract binding to NFKB and GATA dsDNA. There is a massive shift of Hes1 free probe when incubated with the SupT1 nuclear extract, suggesting that the Notch complex is binding to Hes1 dsDNA, but there are no resolved shift bands. There is a possibility that other factors in the nuclear extract, which may or may not be related to Notch, are attributing to the large shift in free probe. The polydI-dC background with the SYBR gold stain (black smearing in the lanes) can also be a limiting factor. To resolve this, a different method of staining, such as radioactive nucleotide labeling, can be employed to provide more sensitivity. Incorporating this method with a longer 4% gel matrix with larger pore sizes might allow for better separation and resolution of the Notch complex.

As the original question of Notch complex binding on the Hes1 SPS cannot be answered from these experiments, purified protein was employed in order to further investigate the Notch signaling system. Purified RBPJ-k was tested for its binding to various Hes1 dsDNA sequences. The three shift bands produced seem to relate to three different protein-DNA complexes binding the WT dsDNA. When removing the ssDNA, one of the shift bands is lost with purified Hes1 dsDNA (Figures 12, 13). These RBPJ-k interactions with ssDNA have never been shown in previous research. The third shift

band is likely to be attributing to RBPJ-k interacting with the ssDNA, which are novel results. Previous data have indicated that DNA-binding proteins do bind ssDNA and have multiple cellular functions (Dickey, Altschuler, & Wuttke, 2013). As a result, this should be further investigated to see whether RBPJ-k has any functional roles when binding ssDNA.

With purified Hes1 dsDNA, it seems that two RBPJ-k complexes are binding, possibly on NRE 2 and 4. When incubating RBPJ-k with NRE 2 or NRE 4 mutants, surprisingly, there is no difference in the shift bands seen when compared to the WT. Even when mutating all the NREs in the Hes1 sequence, the same two shift bands are seen (Figures 14, 15). These results do not comply with previously published data that have shown the MutAB sequence does not shift (Nam et al., 2007). However, these precedented results do not show free probe migration, which makes the data less reliable. This raises the question of whether or not the interactions seen with the mutant dsDNAs are specific, and whether the purified protein concentration is too high. When adding polydI-dC to the RBPJ-k and MutAB incubation, results show the same two protein complexes when comparing the WT to the mutant dsDNA (Figure 16). When titrating out the mutant dsDNA on the right side of the figure, both shift bands are still seen.

Testing fully destructed Hes1 sequences in the presence of polydI-dC did not affect RBPJ-k binding. The restriction digest ends from the destructed mutant were also removed and tested as a binding parameter; no visual difference could be distinguished (Figure 17). Complete destruction of all the NREs within the Hes1 sequence still shifts

RBPJ-k, showing similar binding structures with two distinct shift bands even under optimized conditions.

Previous research has shown that increasing concentrations of NaCl should decrease RBPJ-k interactions with Hes1 dsDNA (Friedmann & Kovall, 2010). Surprisingly enough, increasing the reaction concentration of salt by 450mM did not decrease any binding structures visualized by the shift bands (Figure 18). The higher concentrations of salt should have started to diminish the RBPJ-k + dsDNA shift bands. This suggests that the RBPJ-k interactions witnessed may be something for which we are not be able to control.

Incorporating the same the 5' and 3' ends that were used in previous thermodynamic studies of RBPJ-k (Friedmann & Kovall, 2010) did not produce a difference in shift bands with the mutant dsDNA, which is an NRE 2 mutant. RBPJ-k was then tested for its binding to other DNA sequences not related to Hes1. RBPJ-k is weakly binding to both NFKB and GATA dsDNA (Figures 19, 20). However, only one very light shift band is seen with these short 20bp sequences. This shows that regardless of the sequence, RBPJ-k still has some interactions with the longer DNA sequences, which are seen with Hes1 dsDNA. When shortening the DNA sequence, the interaction is decreased.

To address this, single site NRE and the NRE mutants 17bp long were incubated with RBPJ-k. In the case of the SPS, NRE 2 and NRE 4 binding by RBPJ-k was lost upon mutation of the internal guanines in the NRE (Figure 21), consistent with previous results (Friedmann & Kovall, 2010). One of the shift bands was also lost in the WT dsDNA; this shift band was present in the longer WT sequence with both sites present. This is

expected, as only one RBPJ-k complex can bind to the single site NRE dsDNA. Similar binding results were seen when NRE 3 was tested (Figure 22). Upon mutation of the internal guanines, RBPJ-k binding to NRE 3 was lost. The idea that NRE 3 shows binding raises an interesting question, as RBPJ-k does bind NRE 3 in vitro. However, when considering the Notch dimer architecture, steric hindered might not allow the site to be active in vivo. Previous results have shown that the SPS is required for high promoter functionality. Mutating NRE 3 did not change promoter functionality, and creating a new SPS with NRE 2 and NRE 3 in a head-to-head orientation had a decrease in promoter functionality (Ramos, 2013). NRE 3 has never been shown or identified to have a role in Notch signaling. Despite its context, NRE 3 did show binding in these results, and this is important to note for further studies of RBPJ-k.

Combing the single site NREs in a longer SPS dsDNA shows no visual difference. The same visual binding effect is seen when making the dsDNA longer. It is hypothesized that the binding to the longer dsDNA mutants by RBPJ-k may be a result of the purified RBPJ-k protein interacting with the DNA backbone, as the shorter single site dsDNA showed visual differences. However, it is important to note that in some longer dsDNA mutants, the NRE 3 binding site was still present. As shown by the result here, this could have been contributing to the lower molecular weight shift band seen binding some longer dsDNA mutants.

Previous papers that have shown multiple p53 transcription factors binding to one DNA sequence have suggested that the proteins are interacting with each other (Kearns, Lurz, Orlova, & Okorokov, 2016). This may be plausible for p53, as it is known to form

tetramers. RBPJ-k, however, has never been reported to have such an interaction with itself, so this can likely be ruled out. It is also important to note that the previous studies, which show RBPJ-k does not bind to the SPS mutants (Nam et al., 2007), fail to show the amount of free probe remaining in the shift. Although the binding of RBPJ-k has become better understood, under these conditions, it becomes very difficult to study the protein.

Although the last reported K_D of RBPJ-k was around 1nM, new thermodynamic studies demonstrate that the K_D is actually 100-fold greater at around 100nM. These studies may explain a lesser affinity of RBPJ-k for DNA. The concentration visualized here by the mutant variants was slightly above this amount. With the single site dsDNA, there is a clear difference at 600nM of RBPJ-k, which is more in agreement with the recent reported K_D of 100nM. Other sequences that bind RBPJ-k, such as Hes5, may also be tested and compared for similarities and differences to Hes1.

These results also show there is an interaction with RBPJ-k and the longer dsDNA that we cannot control for; this is likely why the Hes1 mutant dsDNA shifted. When decreasing the size of the dsDNA, we are able to a see a difference in binding structures. This may suggest that RBPJ-k may be a more promiscuous DNA-binding protein than once thought. Based off the purified protein EMSAs, it may be worthwhile to also test the SupT1 nuclear extract with a shorter single site NRE dsDNA that was used with the purified protein, as this may help provide resolved shift bands.

It may be effective to try and control for the other factors binding to Hes1 dsDNA with increased amounts of salt in the reaction mixture, as a high salt content has been shown to decrease protein-DNA interactions. Any unwanted interactions with the SupT1

nuclear extract may be decreased, and this may also provide resolved shift bands. Other methods can also be tried that do not involve EMSA, such as a biotinylated dsDNA pulldown with the SupT1 nuclear extract. Taken together, the difference in structural recruitment of the Notch protein on the SPS versus single NREs on Hes1 needs to be further investigated.

Nevertheless, these results confirm that NRE 2 and NRE 4 of the SPS are required for RBPJ-k binding. Single site dsDNA reveals that the mutation of the internal guanines in in NRE 2, 3, and 4 reduces RBPJ-k binding and produces a significantly different amount of protein-DNA binding structure, which is consistent with the mutations that decreased promoter functionality (Ramos, 2013). Although these internal guanines may not be the only important factors in RBPJ-k binding to its target sequence, they do contribute to a significant amount of binding seen by RBPJ-k. The base pair in between the internal guanine can also represent an important binding factor, as recent results have identified that it has some effect on the binding of RBPJ-k and should be expanded upon (Friedmann & Kovall, 2010).

Mutating the internal guanines in the SPS of the Hes1 gene has been shown to decreases promoter functionality. Here we confirm the structural reduction in RBPJ-k bound to DNA as a result of mutating the internal guanines in the single site NREs. The recruitment of proteins by the NICD-RBPJ-k-MAM ternary complex on the SPS sites has yet to be fully understood. The binding activity of RBPJ-k to ssDNA as well as NRE 3 may suggest there is more information that needs to be uncovered about the protein's selectivity. Alternatively, new research should focus on investigating structure-function

relationships of the SPS and NREs. Providing more information on these topics will aid in our understanding of the Notch pathway and will ultimately provide a target for revolutionary therapeutics in modern medicine. The question about the structural difference of a single, unpaired Notch activation complex as opposed the Notch dimer complex formed on the SPS still remains unanswered. Further studies will be crucial in identifying proteins that may be recruited in vivo by high activation promoters.

References

Arnett, K. L., & Blacklow, S. C. (2014). Analyzing the nuclear complexes of Notch signaling by Electrophoretic Mobility Shift Assay. *Methods in Molecular Biology, 1187,* 231–245. doi: 10.1007/978-1-4939-1139-4_18

Arnett, K. L., Hass, M., McArthur, D. G., Ilagan, M. X., Aster, J. C., Kopan, R., & Blacklow, S. C. (2010). Structural and mechanistic insights into cooperative assembly of dimeric Notch transcription complexes. *Nature Structural & Molecular Biology, 17*(11), 1312–1317. doi: 10.1038/nsmb.1938

Aster J. C., Pear W. S., Blacklow S. C. (2017). The varied roles of Notch in cancer. *Annual Review of Pathology, 12,* 245–275. doi: 10.1146/annurev-pathol-052016-100127

Berezovska, O., Frosch, M., McLean, P., Knowles, R., Koo, E., Kang, D., Shen, J., Lu, F. M., Lux, S. E., Tonegawa, S., & Hyman, B. T. (1999). The Alzheimer-related gene presenilin 1 facilitates notch 1 in primary mammalian neurons. *Brain Research. Molecular Brain Research, 69*(2)*,* 273–280. doi: 10.1016/S0169-328X(99)00119-9

Blackwell, T. K., & Weintraub, H. (1990). Differences and similarities in DNA- binding preferences of MyoD and E2A protein complexes revealed by binding site selection. *Science, 250*(4984)*,* 1104–1110. doi: 10.1126/science.2174572

Blaumueller, C. M., Qi, H., Zagouras, P., & Artavanis-Tsakonas, S. (1997). Intracellular cleavage of Notch leads to a heterodimeric receptor on the plasma membrane. *Cell, 90*(2)*,* 281–291. doi: 10.1016/S0092-8674(00)80336-0

Borggrefe, T. & Oswald, F. (2009). Notch signaling pathway: transcriptional regulation at Notch target genes. *Cellular and Molecular Life Sciences, 66*(10)*,* 1631–1646. doi: 10.1007/s00018-009-8668-7

Bray, S. J. (2006). Notch signaling: a simple pathway becomes complex. *Nature Reviews Molecular Cell Biology, 7*(9)*,* 678–698. doi: 10.1038/nrm2009

Brou, C., Logeat, F., Gupta, N., Bessia, C., LeBail, O., Doedens, J. R., Cumano, A., Roux, P., Black, R. A., & Israel, A. (2000). A novel proteolytic cleavage involved in Notch signaling: the role of the disintegrin-metalloprotease TACE. *Molecular Cell, 5*(2)*,* 207–216. doi: 10.1016/S1097-2765(00)80417-7

Cave, J. W., Loh, F., Surpris, J. W., Xia, L., & Caudy, M. A. (2005). A DNA transcription code for cell-specific gene activation by notch signaling. *Current Biology, 15*(2)*,* 94–104. doi: 10.1016/j.cub.2004.12.070

Collins, K.J., Yuan, Z., & Kovall, R.A. (2014). Structure and function of the CSL-KyoT2 corepressor complex: a negative regulator of notch signaling. *Structure 22*(1), 70–81. doi: 10.1016/j.str.2013.10.010

Cordle, J., Johnson, S., Tay, J. Z. Y., Roversi, P., Wilkin, M., Hernandez-Diaz, B., … & Handford, P. A. (2008). A Conserved Face of the Jagged/Serrate DSL Domain is Involved in Notch Trans-Activation and Cis-Inhibition. *Nature Structural & Molecular Biology, 15*(8)*,* 849–857. doi: 10.1038/nsmb.1457

Crosnier C., Stamataki D., & Lewis J. (2006). Organizing cell renewal in the intestine: Stem cells, signals and combinatorial control. *Nature Reviews Genetics, 7*(5)*,* 349–359. doi:10.1038/nrg1840

D'souza, B., Miyamoto, A., & Weinmaster, G. (2008). The many facets of Notch ligands. *Oncogene, 27*(38)*,* 5148–5167. doi: 10.1038/onc.2008.229

De Strooper, B., Annaert, W., Cupers, P., Saftig, P., Craessaerts, K., Mumm, J. S., Schroeter, E. H., Schrijvers, V., Wolfe, M. S., Ray, W. J., Goate, A., & Kopan, R. (1999). A presenilin-1-dependent gamma-secretase-like protease mediates release of Notch intracellular domain. *Nature, 398*(6727)*,* 518–522. doi: 10.1038/19083

Dexter, J. (1914). The Analysis of a Case of Continuous Variation in Drosophila by a Study of Its Linkage Relations. *The American Naturalist, 48*(576)*,* 712–758. doi: 10.1086/279446

Dickey, T. H., Altschuler, S. E., & Wuttke, D. S. (2013). Single-Stranded DNA-Binding Proteins: Multiple Domains for Multiple Functions. *Structure, 21*(7)*,* 1074–1084. doi: 10.1016/j.str.2013.05.013

Efstratiadis, A., Szabolcs, M., & Klinakis, A., (2007). Notch, Myc and Breast Cancer. *Cell Cycle, 6*(4)*,* 418–429. doi: 10.4161/cc.6.4.3838

Farshbaf, M., Lindberg, M.J., Truong, A., Bevens, Z., Chambers, E., Pournara, A., Wallberg, A., & White, J.B. (2015). Mastermind-Like 1 Is Ubiquitinated: Functional Consequences for Notch Signaling. *PLOS One*, *10*(7)*,* e0134013. doi: 10.1371/journal.pone.0134013

Feder, J. N., Li, L., Jan, L. Y., & Jan, Y. N. (1994). Genomic cloning and chromosomal localization of HRY, the human homolog to the Drosophila segmentation gene, hairy. *Genomics, 20*(1)*,* 56–61. doi: 10.1006/geno.1994.1126

Friedmann, D. R., & Kovall, R. A. (2010).. Thermodynamic and structural insights into CSL-DNA complexes. *Protein Science: A Publication of the Protein Society, 19(*1)*,* 34–46. doi: 10.1002/pro.280

Fryer, C. J., Lamar, E., Turbachova, I., Kintner, C., & Jones, K. A. (2002). Mastermind mediates chromatin-specific transcription and turnover of the Notch enhancer complex. *Genes & Developmental, 16*(11)*,* 1397–1411. doi: 10.1101/gad.991602

Fryer, C. J., White, J. B., & Jones, K. A. (2004). Mastermind recruits CycC:CDK8 to phosphorylate the Notch ICD and coordinate activation with turnover. *Molecular Cell, 16*(4)*,* 509–520. doi: 10.1016/j.molcel.2004.10.014

Gaiano, N., & Fishell, G. (2002). The Role of Notch in Promoting Glial and Neural Stem Cell Fates. *Annual Review of Neuroscience, 25,* 471–490. doi: 10.1146/annurev.neuro.25.030702.130823

Gao, F., Zhang, Y., Wang, S., Liu, Y., Zheng, L., Yang, J., Huang, W., YanFen Ye, Y., Luo, W., & Xiao, D. (2014). Hes1 is involved in the self-renewal and tumourigenicity of stem-like cancer cells in colon cancer. *Scientific Reports, 4,* 3963. doi: 10.1038/srep03963

Gomez-Lamarca, M. J., Falo-Sanjuan, J., Stojnic, R., … Kevin O'Holleran, K., Rhett Kovall, R., & Bray, S.J. (2018). Activation of the Notch Signaling Pathway In Vivo Elicits Changes in CSL Nuclear Dynamics. *Developmental Cell, 44*(5)*,* 611–623.e7. doi: 10.1016/j.devcel.2018.01.020

Hamaguchi, Y., Matsunami, N., Yamamoto, Y., & Honjo, T. (1989). Purification and characterization of a protein that binds to the recombination signal sequence of the immunoglobulin J kappa segment. *Nucleic Acids Research, 17*(22)*,* 9015–9026. Retrieved from https://www.ncbi.nlm.nih.gov/pmc/articles/PMC335110/

Hsieh, J. J., Zhou, S., Chen, L., Young, D. B., & Hayward, S. D. (1999). CIR, a corepressor linking the DNA binding factor CBF1 to the histone deacetylase complex. *Proceedings of the National Academy of Sciences U.S.A., 96*(1)*,* 23–28. doi: 10.1073/pnas.96.1.23

Kageyama R., Ohtsuka T., & Kobayashi T. (2007). The Hes gene family: Repressors and oscillators that orchestrate embryogenesis. *Development, 134,* 1243–1251. doi: 10.1242/dev.000786

Kageyama R., Ohtsuka T., & Kobayashi T. (2008). Roles of Hes genes in neural development. *Developmental Growth & Differentiation, 50*(S1)*,* S97–103. doi: 10.1111/j.1440-169X.2008.00993.x

Kageyama, R., Ohtsuka, T., & Tomita, K. (2000). The bHLH gene Hes1 regulates differentiation of multiple cell types. *Molecules and Cells, 10*(1)*,* 1–7. Retrieved from https://www.ncbi.nlm.nih.gov/pubmed/10774739

Kao, H. Y., Ordentlich, P., Koyano-Nakagawa, N., Tang, Z., Downes, M., Kintner, C. R., Evans, R. M., & Kadesch, T. (1998). A histone deacetylase corepressor complex regulates the Notch signal transduction pathway. *Genes & Developmental, 12*(15)*,* 2269–2277. doi: 10.1101/gad.12.15.2269

Kearns, S., Lurz, R., Orlova, E. V., & Okorokov, A. L. (2016). Two p53 tetramers bind one consensus DNA response element. *Nucleic Acids Research 44*(13), 6185–6199. doi: 10.1093/nar/gkw215

Kodama, Y., Hijikata, M., Kageyama, R., Shimotohno, K., & Chiba, T. (2004). The role of notch signaling in the development of intrahepatic bile ducts. *Gastroenterology, 127*(6)*,* 1775–1786. doi: 10.1053/j.gastro.2004.09.004

Komatsu, H., Chao, M. Y., Larkins-Ford, J., Corkins, M. E., Somers, G. A., Tucey, T., … & Hart, A. C. (2008). OSM-11 Facilitates LIN-12 Notch Signaling during Caenorhabditis elegans Vulval Development. *PLOS Biology, 6*(8)*,* e196. doi: 10.1371/journal.pbio.0060196

Kopan, R. (2012). Notch signaling. *Cold Spring Harbor Perspectives in Biology, 4*(10)*,* pii: a011213. doi: 10.1101/cshperspect.a011213

Kopan, R., & Ilagan, M. X. G. (2009). The Canonical Notch Signaling Pathway: Unfolding the Activation Mechanism. *Cell*, *137*(2)*,* 216–233. doi: 10.1016/j.cell.2009.03.045

Kovall, R. A. (2008). More complicated than it looks: assembly of Notch pathway transcription complexes. *Oncogene, 27*(38)*,* 5099–5109. doi: 10.1038/onc.2008.223

Kovall, R. A. & Blacklow, S. C. (2010). Mechanistic insights into Notch receptor signaling from structural and biochemical studies. *Current Topics in Developmental Biology, 92,* 31–71. doi: 10.1016/S0070-2153(10)92002-4

Kovall, R. A., & Hendrickson, W. A. (2004). Crystal structure of the nuclear effector of Notch signaling, CSL, bound to DNA. *The EMBO Journal, 23*(17)*,* 3441–3451. doi: 10.1038/sj.emboj.7600349

Kovall, R. A., Gebelein, B., Sprinzak, D. & Kopan, R. (2017). Canonical Notch Signaling Pathway: Structural and Biochemical Insights into Shape, Sugar, and Force. *Developmental Cell, 41*(3)*,* 228–241. doi: 10.1016/j.devcel.2017.04.001

Kume, T. (2012). Ligand-Dependent Notch Signaling in Vascular Formation. *Advances in Experimental Medicine & Biology, 727,* 210–222. doi: 10.1007/978-1-4614-0899-4_16

Kurooka H., & Honjo T. (2000). Functional interaction between the mouse notch1 intracellular region and histone acetyltransferases PCAF and GCN5. *Journal of Biological Chemistry, 275*(22)*,* 17211–17220. doi: 10.1074/jbc.M000909200

Laky, K., Evans, S., Perez-Diez, A., & Fowlkes, B. J. (2015). Notch Signaling Regulates Antigen Sensitivity of Naive CD4+ T Cells by Tuning Co-stimulation. *Cell, 42*(1)*,* 80–94. doi: 10.1016/j.immuni.2014.12.027

Lei, L., Xu, A., Panin, V.M., & Irvine, K.D. (2003). An O-fucose site in the ligand binding domain inhibits Notch activation. *Development, 130*(26)*,* 6411–6421. doi: 10.1242/dev.00883

Logeat, F., Bessia, C., Brou, C., LeBail, O., Jarriault, S., Seidah, N. G., & Israel, A. (1998). The Notch1 receptor is cleaved constitutively by a furin-like convertase. *Proceedings of the National Academy of Sciences U. S. A., 95*, 8108–8112. Retrieved from https://www.ncbi.nlm.nih.gov/pmc/articles/PMC20937/

Louvi, A., & Artavanis-Tsakonas, S. (2012). Notch and disease: A growing field. *Seminars in Cell & Developmental Biology*, *23*(4)*,* 473–480. doi: 10.1016/j.semcdb.2012.02.005

Micchelli, C. A., Rulifson, E. J., & Blair, S. S. (1997). The function and regulation of cut expression on the wing margin of Drosophila: Notch, Wingless and a dominant negative role for Delta and Serrate. *Development, 124*(8)*,* 1485–1495. Retrieved from http://dev.biologists.org/content/124/8/1485.long

Moriyama, M., Durham, A. D., Moriyama, H., Hasegawa, K., Nishikawa, S. I., Radtke, F., & Osawa, M. (2008). Multiple Roles of Notch Signaling in the Regulation of Epidermal Development. *Cell, 14(*4)*,* 594–604. doi: 10.1016/j.devcel.2008.01.017

Munro, S., & Freeman, M. (2000). The notch signalling regulator fringe acts in the Golgi apparatus and requires the glycosyltransferase signature motif DXD. *Current Biology, 10*(14)*,* 813–820. doi: 10.1016/S0960-9822(00)00578-9

Murtaugh, L. C., Stanger, B. Z., Kwan, K. M., & Melton, D. A. (2003). Notch signaling controls multiple steps of pancreatic differentiation. *Proceedings of the National Academy of Sciences U. S. A., 100*(25)*,* 14920–14925. doi: 10.1073/pnas.2436557100

Nagel, A.C., Auer, J.S, Schulz, A. Pfannstiel, J., Zhenyu Yuan, Z., Collins, C.E, Kovall, R.A., & Preiss, A. (2017). Phosphorylation of Suppressor of Hairless impedes its DNA-binding activity. *Scientific Reports, 7,* 11820. doi: 10.1038/s41598-017-11952-0

Nam, Y., Sliz, P., Pear, W. S., Aster, J. C., & Blacklow, S. C. (2007). Cooperative assembly of higher-order Notch complexes functions as a switch to induce transcription. *Proceedings of the National Academy of Sciences U. S. A., 104*(7)*,* 2103–2108. doi: 10.1073/pnas.0611092104

Nam, Y., Sliz, P., Song, L., Aster, J. C., & Blacklow, S. C. (2006). Structural basis for cooperativity in recruitment of MAML coactivators to Notch transcription complexes. *Cell, 124*(5)*,* 973–983. doi: 10.1016/j.cell.2005.12.037

Nellesen, D. T., Lai, E. C., & Posakony, J. W. (1999). Discrete enhancer elements mediate selective responsiveness of enhancer of split complex genes to common transcriptional activators. *Developmental Biology, 213*(1), 33–53. doi: 10.1006/dbio.1999.9324

Nobta, M., Tsukazaki, T., Shibata, Y., Xin, C., Moriishi, T., Sakano, S., Shindo, H., & Yamaguchi, A. (2005). Critical Regulation of Bone Morphogenetic Protein-induced Osteoblastic Differentiation by Delta1/Jagged1-activated Notch1 Signaling. *Journal of Biological Chemistry, 280*(16)*,* 15842–15848. doi: 10.1074/jbc.M412891200

Olave, I., Reinberg, D., & Vales, L. D. (1998). The mammalian transcriptional repressor RBP (CBF1). targets TFIID and TFIIA to prevent activated transcription. *Genes & Developmental, 12*(11)*,* 1621–1637. doi: 10.1101/gad.12.11.1621

Ong, C. T., Cheng, H. T., Chang, L. W., Ohtsuka, T., Kageyama, R., Stormo, G. D., & Kopan, R. (2006). Target selectivity of vertebrate notch proteins. Collaboration between discrete domains and CSL-binding site architecture determines activation probability. *Journal of Biological Chemistry, 281*(8)*,* 5106-5119. doi: 10.1074/jbc.M506108200

Oswald, F., Kostezka, U., Astrahantseff, K., Bourteele, S., Dillinger, K., Zechner, U., Ludwig, L., Wilda, M., Hameister, H., Knochel, W., Liptay, S., & Schmid, R. M. (2002). SHARP is a novel component of the Notch/RBP-Jkappa signalling pathway. *The EMBO Journal, 21*(20)*,* 5417-5426. doi: 10.1093/emboj/cdf549

Petcherski A. G., & Kimble J. (2000). LAG-3 is a putative transcriptional activator in the C. elegans Notch pathway. *Nature, 405(*6784)*,* 364–368. doi: 10.1038/35012645

Petcherski A. G., & Kimble J. (2000). Mastermind is a putative activator for Notch. *Current Biology, 10*(13), R471–R473. doi: 10.1016/S0960-9822(00)00577-7

Popko-Scibor, A. E., Lindberg, M. J., Hansson, M. L., Holmlund, T., & Wallberg, A. E. (2011). Ubiquitination of Notch1 is regulated by MAML1-mediated p300 acetylation of Notch1. *Biochemical & Biophysical Research Communications*, *416*(3-4), 300–306. doi: 10.1016/j.bbrc.2011.11.030

Ramos, C., (2013). MASTERMIND-LIKE 1-Dependent Notch Target Gene Activation Requires a Sequence-Paired Site and a TATA Box. *San Jose State University Master's Theses,* 4360. Retrieved from https://scholarworks.sjsu.edu/etd_theses/4360

Sanchez-Irizarry, C., Carpenter, A. C., Weng, A. P., Pear, W. S., Aster, J. C., & Blacklow, S. C. (2004). Notch subunit heterodimerization and prevention of ligand- independent proteolytic activation depend, respectively, on a novel domain and the LNR repeats. *Molecular Cellular Biology, 24*(21), 9265-9273. doi: 10.1128/MCB.24.21.9265-9273.2004

Sasai, Y., Kageyama, R., Tagawa, Y., Shigemoto, R., & Nakanishi, S. (1992). Two mammalian helix-loop-helix factors structurally related to Drosophila hairy and Enhancer of split. *Genes & Developmental, 6*(12B), 2620–2634. doi: 10.1101/gad.6.12b.2620

Schroeter, E. H., Kisslinger, J. A., & Kopan, R. (1998). Notch-1 signalling requires ligand-induced proteolytic release of intracellular domain. *Nature*, *393*(6683), 382–386. doi: 10.1038/30756

Smith, D. R., Myint, T., & Goh, H. S. (1993). Over-expression of the c-myc proto-oncogene in colorectal carcinoma. *British Journal of Cancer, 68*(2), 407–413. Retrieved from https://www.ncbi.nlm.nih.gov/pmc/articles/PMC1968538/

South, A. P., Cho, R. J., & Aster, J. C. (2012). The double-edged sword of Notch signaling in cancer. *Seminars in Cell & Developmental Biology, 23*(4), 458–464. doi: 10.1016/j.semcdb.2012.01.017

Takebayashi, K., Sasai, Y., Sakai, Y., Watanabe, T., Nakanishi, S., & Kageyama, R. (1994). Structure, chromosomal locus, and promoter analysis of the gene encoding the mouse helix-loop-helix factor HES1. Negative autoregulation through the multiple N box elements. *Journal of Biological Chemistry, 269*(7), 5150–5156. Retrieved from http://www.jbc.org/content/269/7/5150.long

Tomita, K., Hattori, M., Nakamura, E., Nakanishi, S., Minato, N., & Kageyama, R. (1999). The bHLH gene Hes1 is essential for expansion of early T cell precursors. *Genes & Development, 13*(9), 1203–1210. Retrieved from http://genesdev.cshlp.org/content/13/9/1203.long

Tun, T., Hamaguchi, Y., Matsunami, N., Furukawa, T., Honjo, T., & Kawaichi, M. (1994). Recognition sequence of a highly conserved DNA binding protein RBP-J kappa. *Nucleic Acids Research, 22*(6), 965–971. Retrieved from https://www.ncbi.nlm.nih.gov/pmc/articles/PMC307916/

VanderWielen, B.D., Yuan, Z., Friedmann, D.R., & Kovall, R.A. (2011). Transcriptional repression in the notch pathway. *Journal of Biological Chemistry, 286*(17), 14892–14902. doi: 10.1074/jbc.M110.181156

Wallberg A.E., Pedersen K., Lendahl U., & Roeder R.G. (2002). p300 and PCAF act cooperatively to mediate transcriptional activation from chromatin templates by notch intracellular domains in vitro. *Molecular Cell Biology 22*(22), 7812–7819.

Weng, A. P., Millholland, J. M., Yashiro-Ohtani, Y., Arcangeli, M. L., Lau, A., Wai, C., … & Aster, J. C. (2006). c-Myc is an important direct target of Notch1 in T-cell acute lymphoblastic leukemia/lymphoma. *Genes & Development, 20,* 2096–2109.

Wilson, J. J., & Kovall, R. A. (2006). Crystal structure of the CSL-Notch- Mastermind ternary complex bound to DNA. *Cell, 124,* 985-996. doi: 10.1128/MCB.22.22.7812-7819.2002

Wolfe, M. S., & Kopan, R. (2007). Presenilin: Running with Scissors in the Membrane. *Cell, 131*(2), 215-221. doi: 10.1016/j.cell.2007.10.012

Wu, L., Aster J. C., Blacklow, S. C., Lake, R., Artavanis-Tsakonas, S., & Griffin, J. D. (2000). MAML1, a human homologue of Drosophila mastermind, is a transcriptional co-activator for NOTCH receptors. *Nature Genetics, 26*(4), 484–489. doi: 10.1038/82644

Xu, A., Haines, N., Dlugosz, M., Rana, N. A., Takeuchi, H., Robert S. Haltiwanger, R. S., & Irvine, K. D. (2007). In Vitro Reconstitution of the Modulation of Drosophila Notch-Ligand Binding by Fringe. *Journal of Biochemistry, 282*(48), 35153-35162. doi: 10.1074/jbc.M707040200

Xu, T., Park, S., Giaimo, B. D., Hall, D., Ferrante, F., Ho, D. M., … Rual, J. (2017). RBPJ/CBF1 interacts with L3MBTL3/MBT1 to promote repression of Notch signaling via histone demethylase KDM1A/LSD1. *The EMBO Journal, 36*(21), 3232–3249. doi: 10.15252/embj.201796525

Yatim, A., Benne, C., Sobhian, B., Laurent-Chabalier, S., Deas, O., Judde, J.-G., … & Benkirane, M. (2012). NOTCH1 Nuclear Interactome Reveals Key Regulators of Its Transcriptional Activity and Oncogenic Function. *Molecular Cell, 48*(3)*,* 445–458. doi: 10.1016/j.molcel.2012.08.022

Zhou, S., & Hayward, S. D. (2001). Nuclear localization of CBF1 is regulated by interactions with the SMRT corepressor complex. *Molecular and Cellular Biology, 21*(18)*,* 6222–6232. doi: 10.1128/MCB.21.18.6222-6232.2001